Linkage-specific ubiquitin chain formation depends on a lysine hydrocarbon ruler

Liwocha, J.; Krist, D.T.; Noort, G.J.V. van; Hansen, F.M.; Truong, V.H.; Karayel, O.; ... ; Schulman, B.A.

ARTICLES
https://doi.org/10.1038/s41589-020-00696-0
nature chemical biology

Check for updates

Linkage-specific ubiquitin chain formation depends on a lysine hydrocarbon ruler

Joanna Liwocha[1,9], David T. Krist[1,8,9], Gerbrand J. van der Heden van Noort[2,9], Fynn M. Hansen[3], Vinh H. Truong[4], Ozge Karayel[3], Nicholas Purser[5], Daniel Houston[5], Nicole Burton[5], Mark J. Bostock[6,7], Michael Sattler[6,7], Matthias Mann[3], Joseph S. Harrison[4], Gary Kleiger[5]✉, Huib Ovaa[2,10]✉ and Brenda A. Schulman[1]✉

Virtually all aspects of cell biology are regulated by a ubiquitin code where distinct ubiquitin chain architectures guide the binding events and itineraries of modified substrates. Various combinations of E2 and E3 enzymes accomplish chain formation by forging isopeptide bonds between the C terminus of their transiently linked donor ubiquitin and a specific nucleophilic amino acid on the acceptor ubiquitin, yet it is unknown whether the fundamental feature of most acceptors—the lysine side chain—affects catalysis. Here, use of synthetic ubiquitins with non-natural acceptor site replacements reveals that the aliphatic side chain specifying reactive amine geometry is a determinant of the ubiquitin code, through unanticipated and complex reliance of many distinct ubiquitin-carrying enzymes on a canonical acceptor lysine.

Ubiquitin (UB) chains are a major post-translational modification controlling protein function in eukaryotic cells. Eight distinct chain types are formed from linkage of the C terminus of one UB to an amino group acceptor (seven lysines and the N terminus) on another UB. The different UB chains form a 'UB code' that is read by cognate binding domains, which control the fates of modified proteins[1–4]. Studies of endogenous and recombinant proteins have shed light on this code, showing that K48-linked chains often direct proteasomal degradation, while K63-linked chains mediate diverse regulation by modulation of multi-subunit complex assembly[1–4]. Structural studies have shown how specificity is determined by the distinct spacing between hydrophobic patches presented by UB molecules linked in various chain types[1–4]. In some cases, the actual isopeptide linkages between the UBs, and the surrounding residues, also dictate recognition of specific UB chains.

Recently, chemical biology approaches have elucidated the principles governing important aspects of UB biology[5]. Indeed, synthetic UB chains with defined linkages and chemically unique properties have highlighted the mechanisms underlying protein degradation by the proteasome[6,7] and revealed the potential of hundreds of UB-binding domains to partner with their cognate chain types[8].

Despite this progress in deciphering how the code is 'read' by the downstream machineries that recognize UB chains, the mechanisms underlying the generation of specific UB chain linkages remain incompletely understood. Chains are forged by combinations of UB-conjugating enzymes (E2s) and UB ligases (E3s). In humans, various pairings among ~30 E2s and ~600 E3s mediate UB ligation to selected target proteins and determine the generation of UB chains with specific linkages. Different E2s and E3s employ distinct enzymatic mechanisms to achieve polyubiquitylation[9,10]. Some E2 enzymes can generate chains themselves, whereby, after enzymatic linkage of the C terminus of a UB to an E2 catalytic cysteine, UB is transferred from the resultant E2~UB intermediate (where ~ refers to a thioester bond) to a lysine on an 'acceptor UB'. The preferred UB acceptor lysine may be intrinsic to an E2 and/or may be influenced by an E2 partner protein[11]. In some cases, UB transfer from the E2 is stimulated by the hallmark 'Really Interesting New Gene' (RING) domain in many E3s. An E2 may also transfer UB to an active-site cysteine of some E3s, as in a 'Homologous to E6AP C-terminus' (HECT) catalytic domain, from which the donor UB is linked to an acceptor UB to generate a chain.

Previous studies have identified E2 or E3 residues that are critical for catalysis and present an acceptor UB to the active site, as well as the roles of acceptor UB residues surrounding the targeted lysine[11–17]. However, whether features of a UB's target lysine beyond its nucleophilic primary amino group—such as the distance between the primary amine and the UB polypeptide backbone—influence UB chain formation remains unknown. Within classes of UB-carrying enzymes (for example, E2 or HECT E3), catalytic domains adopt similar structures that have the capacity to catalyze covalent bond formation between the donor UB and assorted free amino-acid acceptors (lysine, cysteine, serine and threonine)[9,10,18,19]. Because the substrates of the UB system are often degraded even with mutation of the preferred lysines, it seems that targeting by some E2 and E3 enzymes is relatively lax. This contrasts with protein interaction domains or histone-modifying enzymes, which strictly depend on lysines for specific salt-bridge geometries or substrate targeting[20,21].

To investigate whether acceptor lysine side-chain features beyond the primary amino group influence UB chain formation,

[1]Department of Molecular Machines and Signaling, Max Planck Institute of Biochemistry, Martinsried, Germany. [2]Oncode Institute and Department of Cell and Chemical Biology, Chemical Immunology, Leiden University Medical Centre, Leiden, the Netherlands. [3]Department of Proteomics and Signal Transduction, Max Planck Institute of Biochemistry, Martinsried, Germany. [4]Department of Chemistry, University of the Pacific, Stockton, CA, USA. [5]Department of Chemistry and Biochemistry, University of Nevada, Las Vegas, Las Vegas, NV, USA. [6]Biomolecular NMR and Center for Integrated Protein Science Munich at Department Chemie, Technical University of Munich, Garching, Germany. [7]Institute of Structural Biology, Helmholtz Zentrum München, Neuherberg, Germany. [8]Present address: Carle Illinois College of Medicine, Champaign, IL, USA. [9]These authors contributed equally: Joanna Liwocha, David T. Krist, Gerbrand J. van der Heden van Noort. [10]Deceased: Huib Ovaa. ✉e-mail: gary.kleiger@unlv.edu; h.ovaa@lumc.nl; schulman@biochem.mpg.de

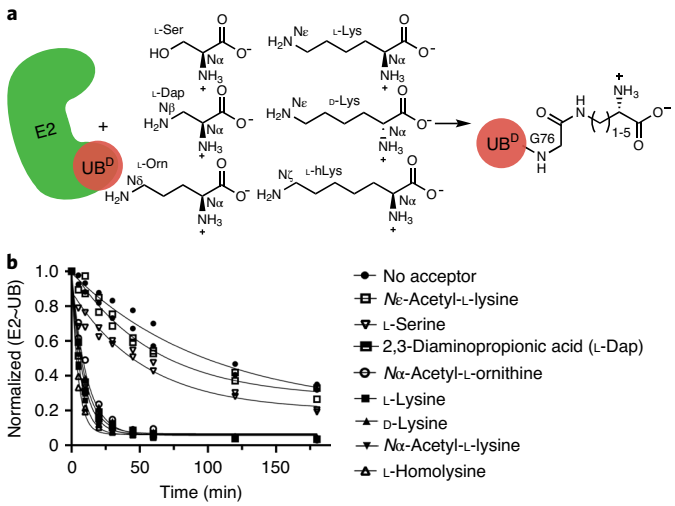

Fig. 1 | UBE2N~UB/UBE2V1/RNF4 RING E3 complex reacts preferentially with free amino acids harboring amine acceptors and various side-chain hydrocarbon linkers. a, Cartoon of the experimental scheme, monitoring the reactivity of E2~UB (D refers to the 'donor' fluorescent UB to be transferred from E2) towards various free amino acids. **b**, Time-course of fluorescent UB discharge from UBE2N~UB/UBE2V1/RNF4 RING E3 to the indicated amino acids, normalized to the starting signal of fluorescent UB thioester-bonded to UBE2N. $N = 2$ independent experiments. For samples derived from the same experiment, gels were processed in parallel.

we employed a suite of synthetic UBs harboring replacements for K11, K48 or K63 with shorter or longer aliphatic side chains, and tested their reactivities with a broad set of ubiquitylating enzymes. Our results demonstrate that the geometry between the polypeptide backbone and primary amine strongly influences chain formation for diverse polyubiquitylating enzymes. Thus, the lysine side chain itself helps establish the UB code.

Results

Acceptor UB lysine geometry required by K63-specific E2. The simplest activity of an E2 involves UB transfer to a nucleophilic amino acid, free in solution. For some E2s, such discharge onto an isolated amino-acid acceptor (for example, lysine, cysteine and threonine) correlates with a preferred residue type modified in the context of a protein target[18,19]. We examined the reactivity of the well-characterized K63-linked UB chain forming enzyme, the human heterodimeric E2 UBE2N/UBE2V1 complex, which uniquely partners a canonical E2 subunit (UBE2N) with the dedicated catalytically inactive E2-like UBE2V1[16,22,23]. UBE2V1 guides K63 (on an acceptor UB) towards the thioester linkage between the active site cysteine of UBE2N and the C terminus of the donor UB[13,22]. The rate of formation of this K63-linked UB chain is accelerated by the RING domain of RNF4 E3 (hereafter referred to as RNF4). RNF4 stabilizes the active conformation of the donor UB thioester-bonded to the UBE2N active site[24]. Moreover, coupling with UBE2V1 and RNF4 stimulates the intrinsic reactivity of the UBE2N~UB intermediate as monitored by UB discharge to free lysine[23], albeit less efficiently than to an acceptor UB's K63.

We examined transfer of the donor UB from RNF4-UBE2V1-activated UBE2N to various free amino acids using a pulse-chase assay (Fig. 1a). UBE2N was charged with fluorescent donor UB in the pulse reaction using E1 enzyme. After quenching this reaction, the resultant UBE2N~UB intermediate was incubated with RNF4, UBE2V1 and an amino acid. We initially tested L-lysine (four methylene units in the side chain, referred to here as C_4) and two controls: L-serine, not known to accept UB from RNF4-UBE2V1-UBE2N, and *N*ε-acetyl-L-lysine, with a blocked ε amino group. As expected, L-lysine had high reactivity compared to controls (Fig. 1b). Reactivity of *N*α-acetyl-L-lysine, with a blocked α amino but available ε amino group, verified lysine's *N*ε-amine as the preferred acceptor. With this established, we tested lysine analogs differing in side-chain length. C_1, C_3 and C_5 analogs (L-2,3-diaminopropionic acid, *N*α-acetyl-L-ornithine and L-homolysine, respectively) demonstrated robust reactivity (Fig. 1b and Extended Data Fig. 1a,b), indicating a lack of an absolute requirement for aliphatic chain length between the backbone and nucleophilic amino group of lysine analogs free in solution.

We next wondered how the L-lysine architecture within the context of an acceptor UB would affect UBE2N/UBE2V1 reactivity (Fig. 2a). Solid-phase peptide synthesis was used to generate five UBs with K63 analogs differing by the number of methylene groups—one, two, three, four or five—between the α carbon and the side-chain amino group: L-2,3-diaminopropionic acid (Dap, referred to here as $^{K63}UB_{C1}$ for one methylene group in the analog replacing native K63), L-2,4-diaminobutyric acid (Dab, referred to here as $^{K63}UB_{C2}$ for two methylene groups in the analog replacing K63), L-ornithine (Orn, referred to here as $^{K63}UB_{C3}$ for three methylene groups in the analog replacing K63), L-lysine (Lys, referred to here as $^{K63}UB_{C4}$ for four methylene groups in the native acceptor) and L-homolysine (hLys, referred to here as $^{K63}UB_{C5}$ for five methylene groups in the analog replacing K63) (Fig. 2b).

UBE2N/UBE2V1 activity was again measured using a pulse-chase assay, with the acceptor now being UB and the product a di-UB chain. Remarkably, unlike in the discharge to free amino acids, removal or addition of only a single methylene from or onto a canonical K63 side chain greatly reduced di-UB chain formation. The striking preference for the native lysine persisted in reactions accelerated by the RNF4 E3 (Fig. 2c).

Lysine geometry impacts many di-UB forming E2s and E3s. Because acceptor UB placement for UBE2N is unique in depending on a partner (UBE2V1)[23], UBE2V1's grip may limit the ability of the reactive amine to reposition in the active site upon addition or removal of a methylene. We thus wondered how changes to the lysine architecture affect other E2s that are reliant on their own surfaces to orient an acceptor UB. Accordingly, we assayed the activities of two K48 linkage-specific E2s, UBE2G1 and UBE2R2, towards a $^{K48}UB_{C1-C5}$ suite[25–27]. Significant di-UB product was only observed with the $^{K48}UB_{C4}$ acceptor—for the E2s alone and for UBE2R2 and UBE2G1 reactions stimulated by cullin-RING ligase E3s CRL1 or CRL4, respectively[25–29], and for substrate-linked acceptors (Fig. 2d). These latter assays depended on CRL receptors recruiting specific substrate degron motifs. The CRL1 receptor FBW7, a tumor suppressor protein, recruits phosphopeptide motifs in targets including the cell cycle regulator cyclin E[30]. For the CRL4 receptor CRBN, the chemotherapeutic agent Pomalidomide induces recognition of zinc finger motifs in neosubstrates including Ikaros family transcription factors[31,32]. $CRL1^{FBW7}$ and $CRL4^{CRBN}$ substrates were generated by sortase-mediated transpeptidation of degron peptides (cyclin E phosphopeptide and IKZF1 zinc finger, respectively) with synthetic UBs. Only native lysine supported substantial UB-chain elongation onto CRL-bound substrates (Fig. 2d).

To determine if the preference for native lysine is preserved for HECT E3 ligases—where UB is transferred from E2 to the HECT catalytic cysteine and then onto the substrate lysine—we assayed the NEDD4 HECT domain[33] and a version of its yeast ortholog Rsp5p harboring substrate-binding WW and catalytic domains[34]. Both forge K63-linked chains[33–35]. Again, robust di-UB formation was only observed with native lysine acceptor $^{K63}UB_{C4}$. Di-UB formation was greatly reduced with $^{K63}UB_{C1-C3}$ or $^{K63}UB_{C5}$, including for a substrate[36] recruited to Rsp5p (Fig. 3a,c).

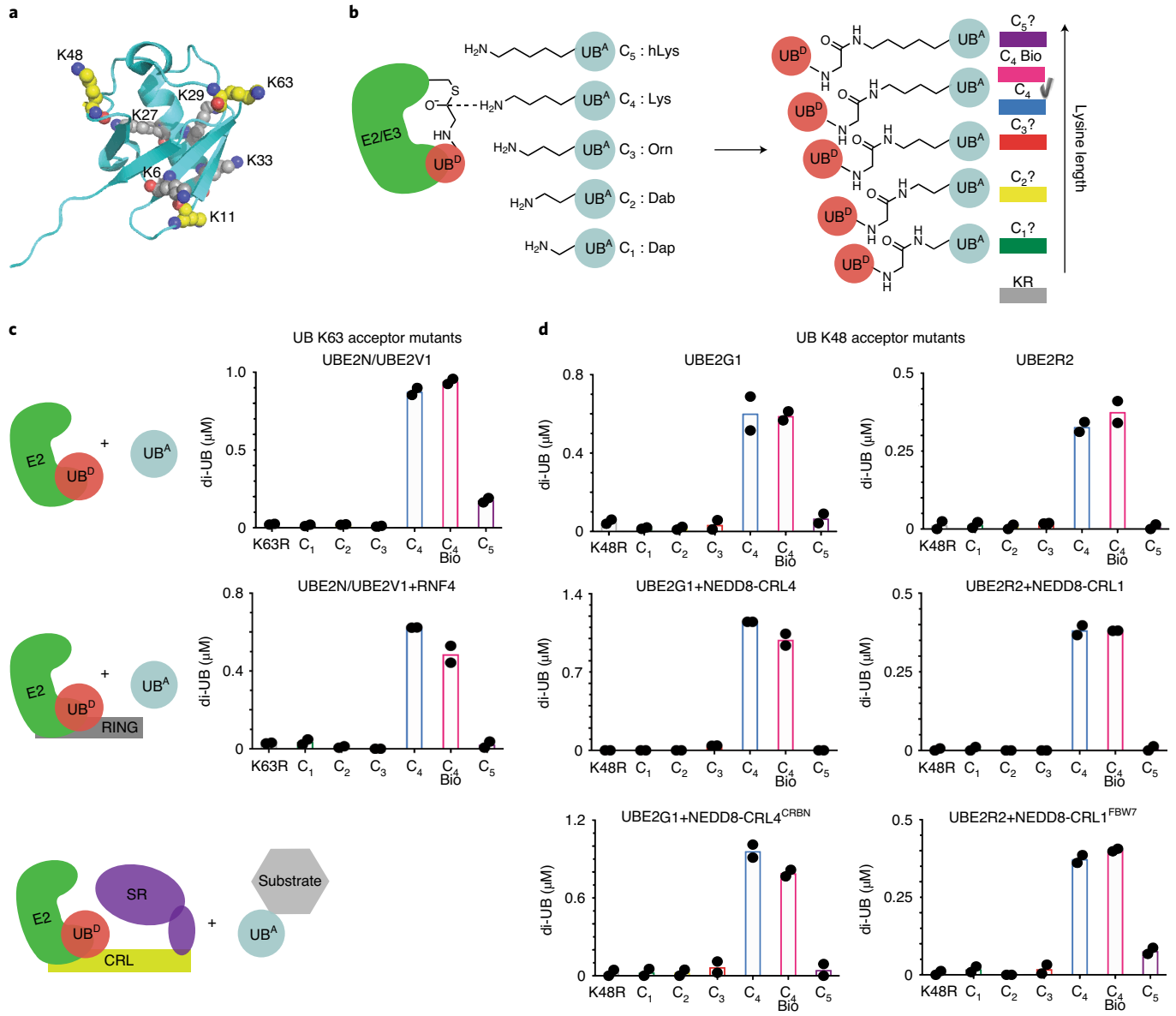

Fig. 2 | K48 and K63 chain-forming E2s show strong preferences for a native lysine acceptor on UB. a, Structure of UB (PDB: 3CMM), showing lysines as spheres and carbon (yellow) and nitrogen (blue) atoms highlighted for K11, K48 and K63 where analogs were installed for this study. **b**, Cartoon of the experimental scheme, monitoring the reactivity of E2-UB (D refers to the fluorescent donor UB to be transferred from E2) and formation of di-UB with various versions of acceptor UB (UB^A). Color coding is used for acceptor lysine analogs denoted as C_1 to C_5 based on having one to five side-chain methylene groups, respectively. KR represents lysine mutation to arginine. **c**, Plots showing the amount of di-UB chain produced by UBE2N/UBE2V1 with UBs harboring the indicated acceptor side chain at position 63 in the absence (top) or presence (bottom) of the E3 RING domain from RNF4. **d**, Plots showing the amount of di-UB chain produced by E2s UBE2G1 and UBE2R2 in the absence (top) or presence (middle) of cognate E3s—NEDD8-CRL4 or NEDD8-CRL1—that activate di-UB synthesis. E2-dependent di-UB forming activity toward E3-bound substrates was tested with substrates (sortase-mediated $^{K48}UB_{C1-C5}$ linked to phospho-cyclin E peptide or IKZF1 ZF 2-3) of neddylated $CRL1^{FBW7}$ or $CRL4^{CRBN}$ (bottom). For all plots, di-UB levels (μM) represent the final time points from the reactions (Source Data Fig. 2), $N = 2$ independent experiments. For samples derived from the same experiment, gels were processed in parallel.

As controls, the $^{K63}UB_{C1-C5}$ analogs served as acceptors with the K48-specific E2 UBE2G1, demonstrating proper folding for the synthetic UBs harboring K63 substitutions (Extended Data Fig. 2a). Similarly, UBE2N/UBE2V1, NEDD4 and Rsp5p also produce nearly wild-type amounts of di-UB chains with UBs harboring lysine analogs on the non-acceptor position 48 ($^{K48}UB_{C1-C5}$, Fig. 3b and Extended Data Fig. 2b). Moreover, proton NMR spectra for recombinant UB ('C_4 Bio'), synthetic UB (aka 'C_4') and $^{K48}UB_{C5}$ showed good dispersion and were superimposable except for a few resonances, presumably reflecting the overall minor impact of sequence differences between them (Met1 in C_4 Bio substituted with NorLeu in synthetic UBs, and Lys48 versus the C_5 side chain, Extended Data Fig. 3).

Taken together, the data show that K63- and K48-specific E2 and E3 enzymes utilizing distinct modes of acceptor UB recruitment display exquisite specificity for the attacking lysine architecture in the context of an acceptor UB. Notably, E2~UB and HECT E3~UB active sites are structurally distinct. Thus, the demand for native

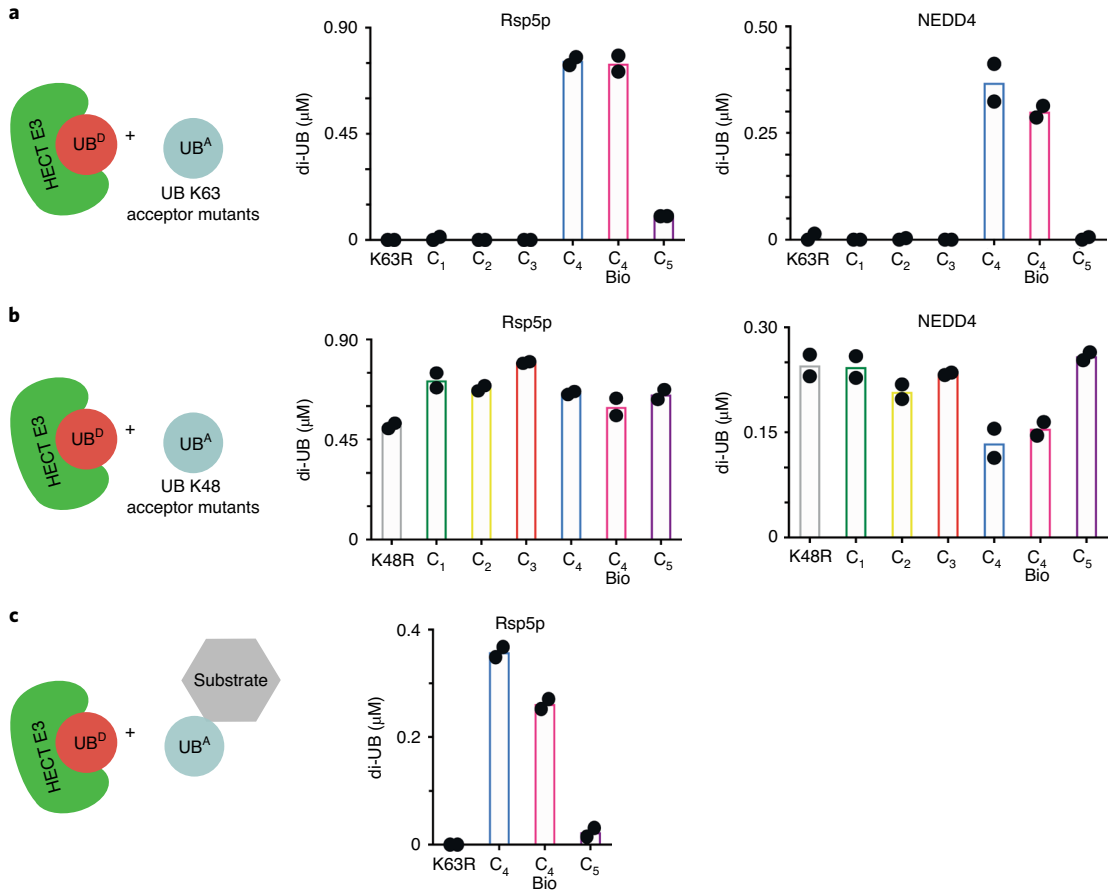

Fig. 3 | K63 chain-forming HECT E3 ligases show strong preferences for a native lysine acceptor on UB. a, Cartoon of the experimental scheme (left) and reactivity of the yeast HECT E3 Rsp5p (middle) or human HECT E3 NEDD4 (right) and formation of di-UB chains with $^{K63}UB_{C1-C5}$ acceptors (UB^A). **b**, Same as in **a**, except with $^{K48}UB_{C1-C5}$ acceptors. **c**, HECT E3 ligase-dependent di-UB forming activity in the context of an Rsp5p-bound substrate (sortase-mediated UB, UB K63R or $^{K63}UB_{C5}$ linkage to the WW-domain-binding PPPY degron motif of the substrate Sna4p). For all plots, di-UB levels (μM) represent the final time points from the reactions (Source Data Fig. 3), $N = 2$ independent experiments. For samples derived from the same experiment, gels were processed in parallel.

lysine acceptor geometry for chain building seems to be a general property that could extend across many of the hundreds of E2/E3 ligation systems.

The K48 side chain impacts the multifunctional E2 UBE2D3. We pondered whether there may be exceptions to linkage-specific ubiquitylation relying on native lysine (C_4) acceptors. The E2 UBE2S, which generates K11 di-UB linkages, is an intriguing candidate, as UBE2S relies on acceptor UB-assisted catalysis[14]. UBE2S displays weak di-UB chain synthesis activity on its own due to the high K_m for the acceptor[14]. This is overcome by fusing a UB-binding domain to UBE2S, or with the anaphase-promoting complex/cyclosome (APC/C) E3, whose RING domain recruits the acceptor UB[37,38]. Results from our qualitative assays suggest that UBE2S is less sensitive to lysine side-chain length, as di-UB formation occurred with $^{K11}UB_{C2-C5}$ acceptors, although $^{K11}UB_{C1}$ was relatively inactive (Extended Data Fig. 4). This is not due to an overt folding defect, as all $^{K11}UB_{C1-C5}$ analogs are acceptors for UBE2N/UBE2V1-dependent K63-linked di-UB formation.

We also examined the relatively promiscuous UB chain-forming enzyme UBE2D3 (also known as UBCH5C): UBE2D3 collaborates with numerous E3s, transfers UB to E3 catalytic cysteines and substrate lysines, generates several UB chain linkages, and forms branched UB chains in multiple turnover polyubiquitylation reactions[39,40]. Pulse-chase assays examining di-UB products of UBE2D3~UB revealed preferential targeting to K11 and K63, according to absolute quantitation by MS (Fig. 4a). However, with a $^{K48}UB_{C5}$ acceptor added to UBE2D3~UB, the SDS–PAGE mobilities of di-UB products differed from those formed with a native UB acceptor. Because different UB chain linkages could impact electrophoretic migration, the result hints at distinct products (Fig. 4b).

We developed a targeted MS strategy to quantify the distributions of UB chain linkages formed with native lysines. Although the method does not detect chains linked to the unnatural amino acid, it quantifies relative UB linkages to the remaining lysines in reactions with $^{K11}UB_{C5}$, $^{K48}UB_{C5}$ or $^{K63}UB_{C5}$ compared to reactions with the C_4 acceptor UB. With $^{K11}UB_{C5}$ or $^{K63}UB_{C5}$ acceptors, UBE2D3~UB generates di-UBs with linkage-type distributions similar to reactions with UB_{C4} (Fig. 4c,d and Extended Data Fig. 5). However, adding an extra methylene group to the side chain at K48 alters the distribution of di-UB species formed. The change between preferred acceptors could be accounted for by two observations. First, there is a relative redistribution from K63 to K11 linkages. Second, although the di-UBs linked via K27, K29 and K33 remain a minor proportion of the total, utilization of these non-preferred acceptors increased compared to UB_{C4}. Thus, the location on UB is a determinant of the requirement for a UB_{C4} by a multifunctional ubiquitylating enzyme.

Impact of side-chain architecture revealed by MD. The potential structural effects of adding a methylene group to the acceptor side

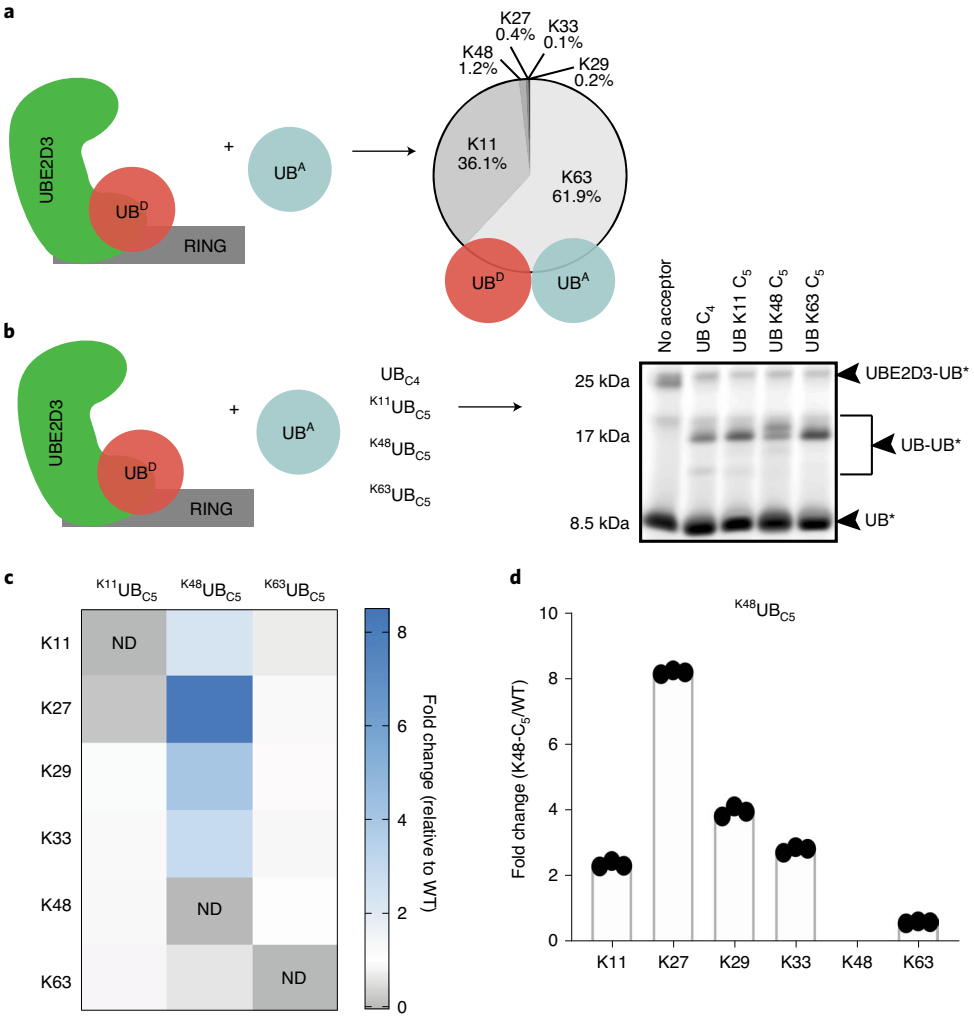

Fig. 4 | The location of lysine analogs on acceptor UB impacts the distribution of di-UB chain linkage types generated by the E2 enzyme UBE2D3. **a**, Cartoon of the experimental scheme and reactivity of UBE2D3-UB (D refers to the donor UB to be transferred from E2) in the presence of the E3 RING domain from RNF4 and formation of di-UB with UB_{C4} acceptor (UB^A). The distribution of the generated di-UB linkage types is shown. **b**, Same as in **a**, except with fluorescent donor UB and various acceptor UBs (UB^A). Notice that di-UB products with distinct electrophoretic mobilities were observed for each acceptor, indicating that the lysine analogs probably affect the di-UB chain linkage identity ($N = 2$ independent experiments). **c**, Relative fold changes of di-UB linkage types for reactions with UBE2D3 and the E3 RING domain from RNF4 comparing $^{K11}UB_{C5}$, $^{K48}UB_{C5}$ or $^{K63}UB_{C5}$ acceptors with UB_{C4}. ND, not defined. **d**, Plot showing the relative changes in UBE2D3/RNF4-generated di-UB chain linkages when comparing products containing $^{K48}UB_{C5}$ or UB_{C4} acceptors. For **c** and **d**, $N = 3$ technical replicates.

chain were revealed by MD simulations on native UB_{C4} or UB_{C5} at position 11, 48 or 63. In two independent 50-ns simulations for UBs with native lysine or C_5 at positions 11, 48 and 63, the overall UB globular fold (residues 1–70) was preserved, with 1.618, 1.271, 1.209 and 1.494 Å average Cα root mean square deviation (RMSD) across the simulations, respectively. Nonetheless, the relative differences for C_5—at all three sites—include (1) an increased potential range of distances between the α carbon and side-chain amine for C_5, with limited overlap in the distribution of relative side-chain amine position (Fig. 5a)—this would effectively impart a greater radius to the C_5 side chain when considering the backbone as the axis of rotation; (2) an expanded number of potential rotamers from 81 to 273, with more accessed by the C_5 side chain in every simulation (C_4:C_5 rotamer ratios for residues 11, 48 and 63 of 56:82, 65:117 and 43:96, respectively); (3) different dynamics for χ angles, particularly χ4, which oscillated more frequently between the three rotamer bins for C_5—this would cause more rapid fluctuation of relative side-chain amine positions (Fig. 5b and Extended Data Fig. 6a). With C_5 at positions 48 and 63, there were also subtle but reproducible increases in fluctuations in the φ and ψ angles (Fig. 5c,d), and an increased number of allowable φ/ψ combinations (C_4:C_5 ratios for residues 11, 48 and 63 of 185:175, 138:169 and 73:90, respectively). Collectively, between the backbone and rotamer combinations, we typically observed more states accessible to the C_5 residue, with a noticeable increase of over 1,000 additional states at positions 48 and 63 (C_4:C_5 ratios at positions 11, 48 and 63 of 2,942:3,016, 2,942:4,261 and 1,188:2,561, respectively).

We wished to further probe the potential effects of the C_5 side chain as an acceptor in di-UB chain formation. The only structurally characterized reaction is a donor UB~UBE2N/UBE2V1/acceptor UB complex, where the acceptor UB's K63 points towards, but is 12.5 Å from, the donor UB's carbonyl to which it becomes linked during di-UB synthesis[23]. Nonetheless, we adapted an intermediate of the acceptor K63 based on modeling and on constraints from enzymology and the crystal structures of wild-type UBE2N/UBE2V1[41,42]. Three independent MD simulations (25 ns each)

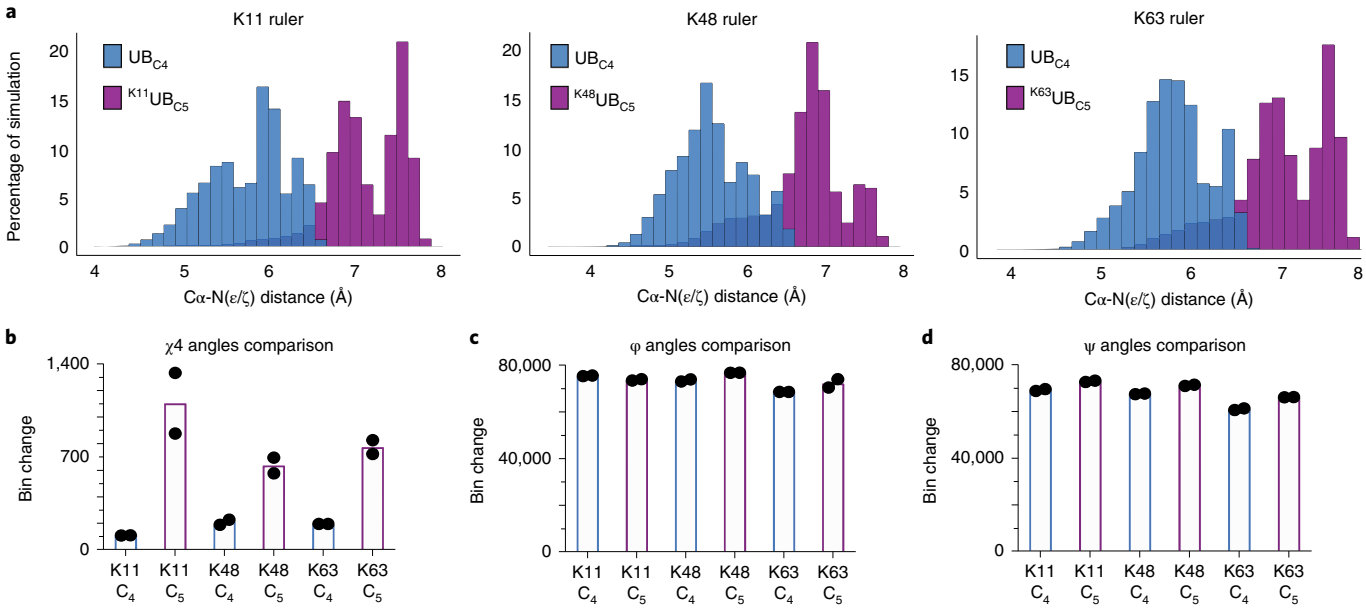

Fig. 5 | Molecular dynamics (MD) simulations reveal pleiotropic structural effects on UBs harboring lysine analogs. a, Distribution of the distances between lysine acceptor amine and Cα atoms for UB_{C4} versus UB_{C5} in MD simulations performed for UB. **b**, Plot showing the dynamics of χ^4 side-chain rotomers for various UB_{C5} acceptors compared with UB_{C4}. Bins are divided by 120° intervals. **c**, Same as in **b**, except for the ψ main-chain torsion angle. Bins are divided by 10° intervals. **d**, Same as in **b**, except for the φ main-chain torsion angle. For all plots, $N = 2$ independent experiments.

showed the C_5 acceptor side chain preferentially adopting extended conformers, and more frequently fluctuating between rotamers, as in the simulations of UB alone. Although both C_4 and C_5 side-chain amines maintained a similar distance to the UBE2N~UB active site (Extended Data Fig. 6b–d), closer inspection revealed two appreciable differences between the simulations: (1) lysine occupied a favorable trajectory towards the active site for a greater proportion of the simulations, whereas C_5 more frequently rotated between rotamer bins and approached the active site from different angles (Extended Data Fig. 6e,f); (2) there was a greater deviation in the conformation of UBE2N's so-called 'active site gate loop' (residues 115–120). Interestingly, this gate loop is important for stabilizing noncovalent interactions between the donor UB tail and UBE2N, configuring catalytic residues and positioning the acceptor lysine relative to the thioester bond for catalysis[41,43]. Distortion of the gate loop conformation, as observed with the C_5 side chain, could reduce the probability of adopting a structure favoring ligation (Extended Data Fig. 6g,h).

Impact of UB acceptor lysine geometry on kinetic parameters. To illuminate mechanistic roles for lysine, quantitative biochemical experiments were performed. Substantially increasing reaction times and protein levels under steady-state conditions enabled quantification for C_5 as acceptor for di-UB formation by the E2s UBE2N/UBE2V1 (with or without RNF4 E3), UBE2R2 and by the HECT E3 Rsp5p.

The reactions with both E2s showed similar profiles overall: k_{cat} values were lower with C_5 replacements for acceptor lysines—16-fold and 14-fold, respectively (Table 1)—consistent with the striking results from the pulse-chase assays (Fig. 2). Although defects in enzyme activity can manifest themselves through various perturbations, failure to activate the acceptor lysine amine or decreasing affinity of the acceptor UB for the E2 are quite common[13,14,44]. A pioneering investigation of the related modification SUMOylation suggested that E2s catalyze ubiquitylation at least in part through the active site complementing the acceptor lysine to achieve pK_a suppression[44]. Despite being unable to estimate apparent pK_a for reactions with E3s due to a loss of enzyme activity at high pH, we were able to determine apparent pK_a values in the reactions with E2s.

UBE2N/UBE2V1 activity (with a K92R mutation to decrease auto-ubiquitylation at high pH[23]) was measured in the presence of $^{K63}UB_{C4}$ or $^{K63}UB_{C5}$ across varying pHs (Table 1 and Extended Data Fig. 7a,b). Although caution should be taken when interpreting apparent pK_a values, because both k_{cat} and K_M may display pH dependencies of their own, the data fit best to a model where a single ionizing species is responsible for the pH dependency of k_{obs} (Extended Data Fig. 7b). Surprisingly, pK_a values were similar in reactions with $^{K63}UB_{C4}$ or $^{K63}UB_{C5}$ (8.9 and 9.0, respectively; Table 1). Parallel experiments with UBE2R2 showed apparent pK_a values of 6.6 and 7.3 for $^{K48}UB_{C4}$ and $^{K48}UB_{C5}$, respectively (Table 1 and Extended Data Fig. 7e). For both E2s, differences in pK_a values are insufficient to account for those between rates of di-UB formation with acceptor lysine or C_5 side chains in reactions at elevated pH (nearly 100-fold for UBE2R2 at pH 9.7, Table 1). The estimated K_M values of $^{K63}UB_{C4}$ or $^{K63}UB_{C5}$ for UBE2N/UBE2V1 were within two-fold, and those of $^{K48}UB_{C4}$ or $^{K48}UB_{C5}$ for UBE2R2 within four-fold, suggesting similar affinities for lysine- and C_5-bearing acceptor UBs and their respective E2s (Table 1 and Extended Data Fig. 7c,f). Thus, defective catalysis seemingly arises from other effects of the additional methylene in the acceptor UB side chain.

An E3 may affect mechanisms underlying acceptor UB lysine specificity. Although the RNF4 RING domain greatly impacted UBE2N/UBE2V1-catalyzed di-UB formation (lowering the K_M of acceptor UB for E2 and increasing k_{cat} by ~17-fold and 11-fold, respectively (Table 1 and Extended Data Fig. 7d)), only modest effects were observed for K_M (~2.5 fold) as well as k_{cat} (~4 fold) in the presence of $^{K63}UB_{C5}$. In combination, these effects are not greater than those observed without E3.

By contrast, kinetic experiments performed on the HECT E3 Rsp5p showed a remarkable 16-fold lower K_M for the acceptor $^{K63}UB_{C4}$ compared with $^{K63}UB_{C5}$, with only a ~2.5-fold difference in

Table 1 | k_{cat}, pK_a^{app} and K_M for UB-carrying enzymes with native versus homolysine acceptor UBs

E2/E3	UB	Lys	pK_a^{app}	k_{obs} (h^{-1}), top pH	K_M (10^{-6} M)	k_{cat} (h^{-1})
UBE2N/V1	C_4 Bio	K63			190	6.1
UBE2N/V1	C_4	K63	8.9	15.8	398	3.4
UBE2N/V1	C_5	K63	9.0	0.58	284	0.21
UBE2N/V1+RNF4	C_4	K63			23	39.1
UBE2N/V1+RNF4	C_5	K63			58	9.3
UBE2R2	C_4	K48	6.6	2.67	528	15.8
UBE2R2	C_5	K48	7.3	0.028	1,940	1.1
Rsp5p	C_4	K63			21	1.11
Rsp5p	C_5	K63			335	0.44

Kinetic parameters for several UB-carrying enzymes, including the apparent pK_a (pK_a^{app}), the rate of di-UB formation (k_{obs}) for UBE2N/UBE2V1 and UBE2R2 at pH 10.1 or 9.7, respectively (k_{obs} (h^{-1}) top pH), and the K_M and k_{cat} of UB_{C4} or UB_{C5} acceptors for E2 or HECT E3. Each value represents the mean of duplicate data points (Source data).

k_{cat} (Table 1 and Extended Data Fig. 7g). Overall, the kinetic results unveil a diverse spectrum of effects of the lysine side-chain ruler on UB-carrying enzyme activities.

Discussion

Our data show that many different UB chain-forming enzymes are strikingly sensitive to the lysine side chain hydrocarbon linker at the ångstrom length scale, as determined by a single methylene. Biochemical assays show that UB_{C5} can affect K_M, k_{cat} and pK_a (Table 1). Meanwhile, MD simulations unveiled pleiotropic structural effects of C_5, including additional degrees of freedom, more side-chain flexibility and more dynamics in the backbone in UB itself (Fig. 5). It might stand to reason that side chains that are too short simply cannot span the distance between the acceptor UB backbone and UB-carrying enzyme active site. However, the fact that the UB_{C5} analogs impacted most tested enzymes indicates further roles of the acceptor side chain.

For both UBE2N/UBE2V1 and UBE2R2, the mild effects on apparent pK_a and/or K_M are insufficient to explain the defects in k_{cat} observed upon acceptor lysine substitution with C_5 (Table 1). The MD simulations pointed towards several possible features of the lysine side-chain length that may be optimal for E2-catalyzed UB chain formation. For example, for enzymes where substrate binding and/or lysine positioning are rate-limiting, it seems that the increased entropy afforded by an extra methylene in the acceptor side chain could decrease the frequency of catalytic encounter (Fig. 5). Interestingly, this mechanism would differ from that of another E2, UBE2W, for which a confluence of disorder between a flexible substrate N terminus and a non-canonical E2 C terminus guides ubiquitylation to a substrate's N-terminal amine[45]. Rather than demanding disorder, the systems tested herein appear to favor a calibrated reach by the nucleophile that also must have restrained degrees of freedom.

In addition to entropic effects on the side chain, the hydrocarbon linker length would also affect catalysis. For example, as shown for UBE2N (without UBE2V1-RING E3 partners), computational studies support a model where there is a precise 'hole' fitting the lysine amine, and attack on the thioester carbonyl is rate-limiting[46]. Our data may suggest that the acceptor UB lysine itself is optimal not only for accessing the amine hole, but also for the chemistry of ubiquitylation. Indeed, the MD simulations of the UB~UBE2N/UBE2V1/UB complex point to multiple ways the acceptor lysine side-chain length could impact catalysis, including through an optimal geometric approach to the active site, and through conformationally toggling the active-site gate loop in the UB~E2 intermediate. Moreover, in agreement with previous studies suggesting this loop in UBE2N essentially closes around the acceptor K63 to promote formation of the transition state[43], our MD simulations showed distortion of the active-site gate loop with the suboptimal C_5 side chain. This would be consistent with UB discharge to free side-chain amine acceptors irrespective of hydrocarbon length, and a dramatic impact on k_{cat} in the context of acceptor UB presented from UBE2V1. One would also predict little impact on K_M in such a case, although lack of an effect on K_M may also reflect that the additional methylene does not impact acceptor UB recruitment to this auxiliary UB-binding domain.

The impact of acceptor side-chain length on the HECT E3 Rsp5p represents the opposite extreme. The predominant effect on K_M implies a role of the acceptor lysine itself in productive binding to the E3. It is possible that local interactions—awaiting elucidation by future structural studies—dominate acceptor UB recruitment[47]. It is also possible that placement of the acceptor lysine in the active site allosterically stabilizes the enzyme~UB conformation that binds the acceptor[48].

Although our study relied on installing side-chain chemical variants, it seems likely that, in the cellular milieu, many natural factors—including linkage within a chain and binding to protein partners—could influence presentation of acceptor lysines resulting in specificity with E2 and E3 enzymes. Strong preferences for the lysine side chain itself may contribute to robust ubiquitylation sufficient to elicit proteasomal degradation, even when preferred targeting sites are unavailable. Such features may also influence the successes or failures of targeted protein degradation strategies that rely on small molecules to direct proteins of therapeutic interest to ubiquitylating enzymes[49,50].

Online content

Any methods, additional references, Nature Research reporting summaries, source data, extended data, supplementary information, acknowledgements, peer review information; details of author contributions and competing interests; and statements of data and code availability are available at https://doi.org/10.1038/s41589-020-00696-0.

Received: 2 April 2020; Accepted: 14 October 2020;
Published online: 7 December 2020

References

1. Dikic, I., Wakatsuki, S. & Walters, K. J. Ubiquitin-binding domains—from structures to functions. *Nat. Rev. Mol. Cell Biol.* **10**, 659–671 (2009).
2. Komander, D. & Rape, M. The ubiquitin code. *Annu. Rev. Biochem.* **81**, 203–229 (2012).
3. Yau, R. & Rape, M. The increasing complexity of the ubiquitin code. *Nat. Cell Biol.* **18**, 579–586 (2016).
4. Kwon, Y. T. & Ciechanover, A. The ubiquitin code in the ubiquitin-proteasome system and autophagy. *Trends Biochem. Sci.* **42**, 873–886 (2017).
5. Mulder, M. P. C., Witting, K. F. & Ovaa, H. Cracking the ubiquitin code: the ubiquitin toolbox. *Curr. Issues Mol. Biol.* **37**, 1–20 (2020).
6. Singh, S. K. et al. Synthetic uncleavable ubiquitinated proteins dissect proteasome deubiquitination and degradation, and highlight distinctive fate of tetraubiquitin. *J. Am. Chem. Soc.* **138**, 16004–16015 (2016).
7. Sun, H. et al. Diverse fate of ubiquitin chain moieties: the proximal is degraded with the target, and the distal protects the proximal from removal and recycles. *Proc. Natl Acad. Sci. USA* **116**, 7805–7812 (2019).
8. Zhang, X. et al. An interaction landscape of ubiquitin signaling. *Mol. Cell* **65**, 941–955 (2017).
9. Buetow, L. & Huang, D. T. Structural insights into the catalysis and regulation of E3 ubiquitin ligases. *Nat. Rev. Mol. Cell Biol.* **17**, 626–642 (2016).
10. Zheng, N. & Shabek, N. Ubiquitin ligases: structure, function and regulation. *Annu. Rev. Biochem.* **86**, 129–157 (2017).

11. Mattiroli, F. & Sixma, T. K. Lysine-targeting specificity in ubiquitin and ubiquitin-like modification pathways. *Nat. Struct. Mol. Biol.* **21**, 308–316 (2014).
12. Bernier-Villamor, V., Sampson, D. A., Matunis, M. J. & Lima, C. D. Structural basis for E2-mediated SUMO conjugation revealed by a complex between ubiquitin-conjugating enzyme Ubc9 and RanGAP1. *Cell* **108**, 345–356 (2002).
13. Eddins, M. J., Carlile, C. M., Gomez, K. M., Pickart, C. M. & Wolberger, C. Mms2–Ubc13 covalently bound to ubiquitin reveals the structural basis of linkage-specific polyubiquitin chain formation. *Nat. Struct. Mol. Biol.* **13**, 915–920 (2006).
14. Wickliffe, K. E., Lorenz, S., Wemmer, D. E., Kuriyan, J. & Rape, M. The mechanism of linkage-specific ubiquitin chain elongation by a single-subunit E2. *Cell* **144**, 769–781 (2011).
15. Smit, J. J. et al. The E3 ligase HOIP specifies linear ubiquitin chain assembly through its RING–IBR–RING domain and the unique LDD extension. *EMBO J.* **31**, 3833–3844 (2012).
16. Berndsen, C. E., Wiener, R., Yu, I. W., Ringel, A. E. & Wolberger, C. A conserved asparagine has a structural role in ubiquitin-conjugating enzymes. *Nat. Chem. Biol.* **9**, 154–156 (2013).
17. Stieglitz, B. et al. Structural basis for ligase-specific conjugation of linear ubiquitin chains by HOIP. *Nature* **503**, 422–426 (2013).
18. Wenzel, D. M., Lissounov, A., Brzovic, P. S. & Klevit, R. E. UBCH7 reactivity profile reveals parkin and HHARI to be RING/HECT hybrids. *Nature* **474**, 105–108 (2011).
19. Pao, K. C. et al. Activity-based E3 ligase profiling uncovers an E3 ligase with esterification activity. *Nature* **556**, 381–385 (2018).
20. Virdee, S., Macmillan, D. & Waksman, G. Semisynthetic Src SH2 domains demonstrate altered phosphopeptide specificity induced by incorporation of unnatural lysine derivatives. *Chem. Biol.* **17**, 274–284 (2010).
21. Temimi, A. H. K. A. et al. Lysine possesses the optimal chain length for histone lysine methyltransferase catalysis. *Sci. Rep.* **7**, 16148 (2017).
22. McKenna, S. et al. Noncovalent interaction between ubiquitin and the human DNA repair protein Mms2 is required for Ubc13-mediated polyubiquitination. *J. Biol. Chem.* **276**, 40120–40126 (2001).
23. Branigan, E., Plechanovová, A., Jaffray, E. G., Naismith, J. H. & Hay, R. T. Structural basis for the RING-catalyzed synthesis of K63-linked ubiquitin chains. *Nat. Struct. Mol. Biol.* **22**, 597–602 (2015).
24. Branigan, E., Carlos Penedo, J. & Hay, R. T. Ubiquitin transfer by a RING E3 ligase occurs from a closed E2~ubiquitin conformation. *Nat. Commun.* **11**, 2846 (2020).
25. Petroski, M. D. & Deshaies, R. J. Mechanism of lysine 48-linked ubiquitin-chain synthesis by the cullin–RING ubiquitin–ligase complex SCF–Cdc34. *Cell* **123**, 1107–1120 (2005).
26. Choi, Y.-S. et al. Differential ubiquitin binding by the acidic loops of Ube2g1 and Ube2r1 enzymes distinguishes their Lys-48-ubiquitylation activities. *J. Biol. Chem.* **290**, 2251–2263 (2015).
27. Hill, S., Harrison, J. S., Lewis, S. M., Kuhlman, B. & Kleiger, G. Mechanism of Lysine 48 selectivity during polyubiquitin chain formation by the Ube2R1/2 ubiquitin-conjugating enzyme. *Mol. Cell. Biol.* **36**, 1720–1732 (2016).
28. Lu, G. et al. UBE2G1 governs the destruction of cereblon neomorphic substrates. *eLife* **7**, e40958 (2018).
29. Hill, S. et al. Robust cullin–RING ligase function is established by a multiplicity of poly-ubiquitylation pathways. *eLife* **8**, e51163 (2019).
30. Skaar, J. R., Pagan, J. K. & Pagano, M. Mechanisms and function of substrate recruitment by F-box proteins. *Nat. Rev. Mol. Cell Biol.* **14**, 369–381 (2013).
31. Kronke, J. et al. Lenalidomide causes selective degradation of IKZF1 and IKZF3 in multiple myeloma cells. *Science* **343**, 301–305 (2014).
32. Lu, G. et al. The myeloma drug lenalidomide promotes the cereblon-dependent destruction of Ikaros proteins. *Science* **343**, 305–309 (2014).
33. Maspero, E. et al. Structure of a ubiquitin-loaded HECT ligase reveals the molecular basis for catalytic priming. *Nat. Struct. Mol. Biol.* **20**, 696–701 (2013).
34. Kamadurai, H. B. et al. Mechanism of ubiquitin ligation and lysine prioritization by a HECT E3. *eLife* **2**, e00828 (2013).
35. Kim, H. C. & Huibregtse, J. M. Polyubiquitination by HECT E3s and the determinants of chain type specificity. *Mol. Cell. Biol.* **29**, 3307–3318 (2009).
36. Gupta, R. et al. Ubiquitination screen using protein microarrays for comprehensive identification of Rsp5 substrates in yeast. *Mol. Syst. Biol.* **3**, 116 (2007).
37. Bremm, A., Freund, S. M. V. & Komander, D. Lys11-linked ubiquitin chains adopt compact conformations and are preferentially hydrolyzed by the deubiquitinase Cezanne. *Nat. Struct. Mol. Biol.* **17**, 939–947 (2010).
38. Brown, N. G. et al. Dual RING E3 architectures regulate multiubiquitination and ubiquitin chain elongation by APC/C. *Cell* **165**, 1440–1453 (2016).
39. Brzovic, P. S. & Klevit, R. E. Ubiquitin transfer from the E2 perspective: why is UbcH5 so promiscuous? *Cell Cycle* **5**, 2867–2873 (2006).
40. Swatek, K. N. et al. Insights into ubiquitin chain architecture using Ub-clipping. *Nature* **572**, 533–537 (2019).
41. Lee, B. L., Singh, A., Mark Glover, J. N., Hendzel, M. J. & Spyracopoulos, L. Molecular basis for K63-linked ubiquitination processes in double-strand DNA break repair: a focus on kinetics and dynamics. *J. Mol. Biol.* **429**, 3409–3429 (2017).
42. Garg, P. et al. Structural and functional analysis of ubiquitin-based inhibitors that target the backsides of E2 enzymes. *J. Mol. Biol.* **432**, 952–966 (2020).
43. Rout, M. K. et al. Stochastic gate dynamics regulate the catalytic activity of ubiquitination enzymes. *J. Am. Chem. Soc.* **136**, 17446–17458 (2014).
44. Yunus, A. A. & Lima, C. D. Lysine activation and functional analysis of E2-mediated conjugation in the SUMO pathway. *Nat. Struct. Mol. Biol.* **13**, 491–499 (2006).
45. Vittal, V. et al. Intrinsic disorder drives N-terminal ubiquitination by Ube2w. *Nat. Chem. Biol.* **11**, 83–89 (2015).
46. Jones, W. M., Davis, A. G., Wilson, R. H., Elliott, K. L. & Sumner, I. A conserved asparagine in a ubiquitin-conjugating enzyme positions the substrate for nucleophilic attack. *J. Comput. Chem.* **40**, 1969–1977 (2019).
47. Wang, M., Cheng, D., Peng, J. & Pickart, C. M. Molecular determinants of polyubiquitin linkage selection by an HECT ubiquitin ligase. *EMBO J.* **25**, 1710–1719 (2006).
48. Scott, D. C. et al. Structure of a RING E3 trapped in action reveals ligation mechanism for the ubiquitin-like protein NEDD8. *Cell* **157**, 1671–1684 (2014).
49. Burslem, G. M. & Crews, C. M. Proteolysis-targeting chimeras as therapeutics and tools for biological discovery. *Cell* **181**, 102–114 (2020).
50. Verma, R., Mohl, D. & Deshaies, R. J. Harnessing the power of proteolysis for targeted protein inactivation. *Mol. Cell* **77**, 446–460 (2020).

Methods

Constructs, protein expression and purification. All expression constructs were prepared using standard molecular biology methods. Modifications to protein amino-acid sequences were accomplished using PCR and the Quikchange mutagenesis kit (Agilent). The human E2 constructs used in this study are Glutathione S-transferase (GST)-Tobacco Etch Virus Protease (TEV)-UBE2R2, GST-TEV-UBE2N, GST-TEV-UBE2N harboring a K92R mutation, GST-TEV-UBE2D2, GST-TEV-UBE2D3, His-GST-Ps3C-UBE2V1, UBE2G1-TEV-His and GST-TEV-UBE2S (1–196) fused with the human USP5/IsoT (residues 173–289) domain—here called UBE2S_IsoT[37]. Human HECT E3 ligase NEDD4 was expressed as a GST-TEV-NEDD4 construct, and yeast HECT E3 Rsp5p containing residues 383-C (with WW-domain-binding PPPY degron motif of the substrate Sna4p) was expressed as a GST-TEV-Rsp5p construct[34]. All E2s, both HECT E3s and His-sortase A were expressed in BL21-Gold(DE3) bacterial cells. Proteins were purified by either GST or nickel affinity chromatography and cleaved on beads overnight with TEV or 3C protease. Cleaved protein solutions were then subjected to ion exchange chromatography followed by size exclusion chromatography in 25 mM HEPES pH 7.5, 150 mM NaCl and 1 mM DTT buffer. Human SKP1-FBW7 complex, NEDD8, APPBP1-UBA3 (the E1 to activate NEDD8), UBE2M (a NEDD8 E2-conjugating enzyme) and fluorescently labeled wild-type, K11R, K48R or K63R UB were generated as previously described[48,51,52]. APC/C and CDH1 were expressed and purified as previously described[53]. The RING–RING fusion version of RNF4 was expressed and purified as previously described[54]. Coding regions for CUL1, CUL4A (38-C), RBX1 (5-C) His-TEV-DDB1, CRBN, GST-TEV-IKZF1 (encompassing zinc fingers 2–3 containing amino acids 141–243$_{\Delta 197-238}$; referred to as IKZF1 ZF 2–3)[55] and UBA1 were all subcloned into pLIB vectors[56]. Baculoviruses for CUL1, GST-TEV-RBX1 5-C, CUL4A 38-C, HIS-TEV-DDB1 and CRBN were first prepared and isolated from Sf9 cells, followed by CUL1 and GST-TEV-RBX1 5-C, CUL4A 38-C and GST-TEV-RBX1 5-C, HIS-TEV-DDB1 and CRBN co-infection of Hi5 cells for co-expression[51,52]. Proteins were purified by His or GST affinity chromatography followed by overnight TEV cleavage. Cleaved protein solutions were then subjected to ion exchange chromatography followed by size exclusion chromatography in 25 mM HEPES pH 7.5, 150 mM NaCl and 1 mM DTT buffer. The covalent modification of CUL1-RBX1 (CRL1) and CUL4A-RBX1 (CRL4) with the CRL activator protein NEDD8 (termed neddylation) was performed as previously described[51,52,57]. All variants of UB used in this study were generated as previously described[53].

A plasmid for the bacterial expression of K63R human UB was prepared by using a previous construct for a GST fusion[58] to wild-type human UB containing a consecutive N-terminal TEV cleavage site (ENLYFQG) and protein kinase A consensus sequence (RRASVG) for radiolabeling. Mutation of K63 to Arg was accomplished by the Quikchange method, using DNA oligo sequences 5′-GATTACAACATTCAGAGGGAGTCCACCTTACATC-3′ for the forward primer and 5′-GATGTAAGGTGGACTCCCTCTGAATGTTGTAATC-3′ for the reverse one. The construct DNA sequence was validated by Sanger sequencing. The plasmid was transformed into chemically competent BL21(DE3) *Escherichia coli* bacteria for expression at 37 °C. Protein purification was accomplished using standard approaches[58], with the final step being gel filtration chromatography into a buffer containing 30 mM Tris, pH 8.0, 100 mM NaCl, 1 mM DTT and 10% glycerol. Purified K63R UB was concentrated to ~250 μM based on an extinction coefficient of 1,280 M^{-1} cm^{-1} and flash frozen in liquid nitrogen before storage at −80 °C. K63R UB (50 or 100 μM) was radiolabeled in the presence of 5 kU of cyclic adenosine monophosphate-dependent protein kinase (New England Biolabs) and [γ^{32}P]-adenosine triphosphate (ATP) for 1 h at 30 °C.

All UB-conjugating enzymes (E2s) and their associated E3s employed in this study are listed in Supplementary Table 1.

Donor UB discharge assay (pulse-chase) to free amino acids. UBE2N (20 μM) was loaded with 20 μM fluorescent UB K63R (UB*) in the presence of 0.3 μM UBA1 in buffer containing 50 mM Hepes, pH 7.5, 100 mM NaCl, 2.5 mM $MgCl_2$, 1.5 mM ATP and 0.05 mg ml^{-1} BSA. Loading reactions were incubated for 0.5 h and quenched by adding EDTA to a final concentration of 30 mM. The reaction was then initiated by adding UBE2N~UB* (0.5 μM final) to a substrate mix containing 0.5 μM UBE2V1, 0.5 μM RNF4 RING domain and 35 mM amino-acid acceptors (N_ε-acetyl-L-lysine, L-serine, L-Dap, $N\alpha$-acetyl-L-ornithine, L-lysine, D-lysine, $N\alpha$-acetyl-L-lysine or L-homolysine). Reactions were quenched with either non-reducing or reducing SDS–PAGE sample buffer after 0, 5, 10, 20, 30, 45, 60, 120 or 180 min, and substrates and products were separated by SDS–PAGE. Gels were scanned on an Amersham Typhoon system (GE Healthcare) and the intensities of all fluorescent bands were quantified using ImageQuantTL (GE Healthcare). The E2~UB* band intensities were divided by the total fluorescent intensity in each lane and normalized to the 0 time point. Data were plotted in GraphPad Prism 8 (GraphPad Software) and fitted to an exponential decay function using nonlinear regression (Fig. 1 and Extended Data Fig. 1). All reactions were performed in duplicate. Source Data Fig. 1 and Source Data Extended Data Fig. 1 contain all gels obtained from this experiment.

Transpeptidation reactions. Sortase-mediated transpeptidation was utilized to link the C terminus of various acceptor UBs to the N terminus of a cyclin E phosphopeptide (Nterm-GGGGLPSGLL(pT)PPQ(pS) GKKQSSDYKDDDDK-Cterm), IKZF1 ZF 2–3 or Sna4p peptide (Nterm-GGGGQSLVESPPPYVPENLYFQGDYKDDDDK-Cterm). UBs were synthesized or expressed recombinantly that contained a G76S mutation followed by the GSGSLPETGG sortase recognition sequence. Briefly, 50 μM UB was mixed with 100 μM substrate and 10 μM His-sortase on ice in a buffer containing 50 mM Tris, pH 8.0, 150 mM NaCl, 10 mM $CaCl_2$ for 1 h. Next, the reaction mixture was exposed to nickel-agarose beads to remove His-sortase. Final products were purified by size exclusion chromatography in 25 mM HEPES pH 7.5, 150 mM NaCl and 1 mM DTT buffer. For the UB-Sna4p fusions, an additional overnight incubation with TEV was included to remove a FLAG tag from Sna4p peptide, followed by size exclusion chromatography.

Donor UB discharge assay (pulse-chase) to UB analogs. E2s (20 μM) were loaded with 20 μM fluorescent donor UB (UB*) to form the E2–UB* complex in the presence of 0.3 μM UBA1 in a buffer containing 50 mM Hepes, pH 7.5, 100 mM NaCl, 2.5 mM $MgCl_2$, 1.5 mM ATP and 0.05 mg ml^{-1} BSA. Loading reactions were quenched with EDTA (30 mM final) after a 0.5-h incubation period at room temperature. Reactions were initiated by the addition of various UB acceptors, and in some cases E3s (Supplementary Tables 2–4 report the final concentrations of these reagents for all pulse-chase reactions) in a buffer containing 25 mM Hepes, pH 7.5, 150 mM NaCl together with E2–UB* (~0.5 μM final). All reactions were performed at room temperature for the indicated times and quenched with non-reducing SDS–PAGE sample buffer. Substrates and products were separated by SDS–PAGE and scanned on an Amersham Typhoon system (GE Healthcare). The intensities of all fluorescent bands were quantified using ImageQuantTL (GE Healthcare).The amount of di-UB chain was calculated by first dividing the di-UB* band intensity by the total UB* intensity in each lane of the gel. The fraction of di-UB* product was then multiplied by the total amount of UB* (μM) used in the reactions. All reactions were performed in duplicate.

For UBE2S, donor UB can be transferred to a lysine on the E2 surface (termed autoubiquitination). To minimize this, E1~UB* was prepared and added to UBE2S protein immediately before initiation of the reaction. Briefly, 10 μM UBA1 was first loaded with 20 μM UB* at room temperature for 0.5 h. E1–UB* was desalted twice, using a Zeba desalting column, to quench loading into a buffer containing 25 mM HEPES pH 7.5 and 150 mM NaCl. Reactions were initiated as described above by the addition of UB acceptors and UBE2S with APC/C and its coactivator CDH1 to achieve final concentrations of ~5 μM E1–UB* and 0.2 μM E2. Reactions were processed as described above.

For reactions containing CRL1-bound substrate, the SKP1/FBW7 substrate receptor was utilized to reconstitute the full CRL ($CRL1^{FBW7}$), which binds to phosphorylated cyclin E peptide. For reactions containing CRL4-bound substrate, the substrate adapter CRBN was utilized to reconstitute the full CRL ($CRL4^{CRBN}$). Here, the small molecule pomalidomide (2 μM final) facilitates complex formation between the sortased IKZF1 ZF 2–3-UB fusion and $CRL4^{CRBN}$. All reactions for CRL-bound substrates had an approximate final concentration of 0.5 μM E2~UB that had been generated in the pulse step. All CRL-dependent reactions were processed as described above. Source Data Figs. 2 and 3 and Source Data Extended Data Figs. 2 and 4 contain all gels obtained from this experiment.

In-gel digestion protocol for liquid chromatography–tandem mass spectrometry. UBE2D3 pulse-chase reactions were run as described above (see biochemical assay section). Briefly, UBE2D3 was loaded with either fluorescently labeled UB (UB*) or GST-UB. Note that GST-tagged donor UB was used to separate di-UB^D, which is formed during the pulse reaction as a side product, from the desired di-UB product between donor and acceptor UBs. Chase reactions contained 1 μM RNF4 and 100 μM UB_{C4}, $^{K11}UB_{C5}$, $^{K48}UB_{C5}$ or $^{K63}UB_{C5}$. After a 15-min incubation for UB_{C4} or 1 h for UB_{C5}, reactions were quenched with SDS–PAGE sample buffer. Reactants and products were separated by SDS–PAGE. Gels with samples containing UBE2D3-UB* were scanned on an Amersham Typhoon system (GE Healthcare) and used to generate the image in Fig. 4b. Gels with samples containing UBE2D3-GST-UB were first stained with Coommassie brilliant blue to identify and excise the desired GST-UB^D-UB^A product band. After staining, the gel was subsequently destained by soaking for several hours in 10% acetic acid, 40% methanol and 60% de-ionized water with at least two changes of the solvent to achieve a clear background. The gel band corresponding to GST-UB^D-UB^A was excised and chopped into smaller pieces (~1 × 1 mm). Gel pieces were washed twice with 50% 50 mM ammonium bicarbonate, pH 8.0 (ABC)/50% EtOH and then completely dehydrated by incubation in absolute EtOH. The gel pieces were then dried in a Speed-vac system (Eppendorf, Concentrator plus), rehydrated in 200 μl of 1% (wt/vol) Sodium deoxycholate (SDC) buffer (10 mM Tris-(2-carboxyethyl)phosphine (TCEP), 40 mM 2-chloroacetamide (CAA), 0.5 μg trypsin, 0.5 μg LysC in 100 mM Tris-HCl pH 8.5) and incubated at 37 °C overnight. The next day, peptides were extracted from gel pieces by two consecutive rounds of adding isopropanol buffer (1% 2,2,2-trifluoroacetic acid (TFA) in isopropanol) to the samples and subsequent collection of the liquid phase. At this step, stable isotope-labeled (SIL) analogs of chain specific native di-Gly peptide standards were added to the samples, which provided chromatographic orientation for the detection of endogenous (light)

counterparts. For absolute quantification of different di-Gly peptides in UB_{C4} samples, SIL analog spike-in amounts were adjusted to yield peptide quantification ratios between 0.1 and 10 (20 and 2 fmol per injection for K11_GG, K48_GG, K63_GG and K27, K29, K33, respectively).

Liquid chromatography–tandem mass spectrometry sample preparation. Stage Tips were prepared by inserting three layers of an Styrenedivinylbenzene-reverse phase sulfonate (SDB-RPS) matrix (Empore) into a pipette tip using an in-house prepared syringe device as described previously[59,60]. The peptides, mixed with isopropanol buffer, were loaded onto the StageTips. The tips were washed with isopropanol buffer and subsequently with 2% ACN/0.2% TFA. Elution was performed using 80% ACN/1.25% NH_4OH. Eluates were collected in PCR tubes and dried using a Speed-vac centrifuge. Peptides were resuspended in buffer A* (2% ACN/0.2% TFA) and briefly sonicated (Branson Ultrasonics) before LC/MS-MS analysis.

Liquid chromatography–tandem mass spectrometry measurements. Peptides were loaded on a 50-cm reversed-phase column (75 µm inner diameter, packed in house with ReproSil-Pur C18-AQ 1.9-µm resin (Dr Maisch)). The column temperature was maintained at 60 °C using a homemade column oven. An EASY-nLC 1200 system (Thermo Fisher Scientific) was directly coupled online with the mass spectrometer (Q Exactive HF-X, Thermo Fisher Scientific) via a nano-electrospray source, and peptides were separated with a binary buffer system of buffer A (0.1% formic acid (FA)) and buffer B (80% acetonitrile, 0.1% FA), at a flow rate of 300 nl min^{-1}. Peptides were eluted with a gradient starting at 7% buffer B (0.1% (vol/vol) FA, 80% (vol/vol) ACN) and stepwise increased to 14% in 4 min and 26% in 22 min. After each gradient, buffer B concentration was increase to 95% in 2 min and maintained at this concentration for 6 min.

The mass spectrometer was programmed to acquire in targeted scan mode in which every full scan, with resolution of 60,000 at 200 m/z (3×10^6 ions accumulated with a maximum injection time of 20 ms), was followed by 20 multiplexed selected ion monitoring (SIM) scans employing a multiplexing degree of four. Light (endogenous) and heavy counterpart peptides were always simultaneously recorded in the same scan. Each SIM scan covered a range of m/z of 150–2,000 with resolution of 120,000 (5×10^4 ions accumulated with a maximum injection time of 65 ms, 1.4-m/z isolation window and 0.4-m/z isolation offset). The targeted peptides with m/z values are listed in Supplementary Table 5.

Data analysis. Raw MS data were processed using Skyline, an open-source software project[57,58]. Graphical displays of chromatographic traces were manually inspected for proper peak picking of MS1 filtered endogenous peptides based on co-eluting SIL peptides. All quantification was done on the precursor ion level, based on area. Only the most abundant peak of the isotope cluster was used for quantitation.

Bioinformatics analyses in this study were performed with Microsoft Excel and data visualized using GraphPad Prism (GraphPad Software). The background signal detected in the sample lacking acceptor UB was substracted from the corresponding signals of samples containing acceptor UBs. Next, each chain peptide was normalized to the first tryptic peptide of the N-terminally modified UB^{A} (M1Nle) sequence: 'NleQIFVK'. Because this peptide was used for normalization, K6-linked di-UB was not measured in our protocol. Finally, fold changes of each chain peptide (relative to WT) are calculated using the equations in the next section and shown in Fig. 4c,d and Extended Data Fig. 5a,b. All gels used in this experiment are shown in Source Data Fig. 4.

Equations. Correction for background signal by subtraction of signal detected in 'no acceptor' reactions:

$$\mathrm{AUC}_{\mathrm{rep}\,i}^{\mathrm{UB^{Acceptor,BGcorr}}} = \mathrm{AUC}_{\mathrm{rep}\,i}^{\mathrm{UB^{Acceptor}}} - \overline{\mathrm{AUC}}^{\mathrm{UB^{no\ Acceptor}}} \{i | 1 \le i \le 3\} \quad (1)$$

Normalization of GlyGly peptides to NleQIFVK:

$$_{\mathrm{GG-Pep.}}\mathrm{AUC}_{\mathrm{rep}\,i}^{\mathrm{UB^{Acceptor,Norm}}} = \frac{_{\mathrm{GG-Pep.}}\mathrm{AUC}_{\mathrm{rep}\,i}^{\mathrm{UB^{Acceptor,BGcorr}}}}{_{\mathrm{NleQIFVK}}\mathrm{AUC}_{\mathrm{rep}\,i}^{\mathrm{UB^{Acceptor,BGcorr}}}} \{i | 1 \le i \le 3\} \quad (2)$$

Foldchange calculation of UB_{C5} to UB_{C4}:

$$_{\mathrm{GG-Pep.}}\mathrm{FC}_{\mathrm{rep}\,i}^{\mathrm{UB^{Acceptor,Norm}}} = \frac{_{\mathrm{GG-Pep.}}\mathrm{AUC}_{\mathrm{rep}\,i}^{\mathrm{UB_{C5}^{Acceptor,Norm}}}}{_{\mathrm{GG-Pep.}}\widetilde{\mathrm{AUC}}^{\mathrm{UB_{C4}^{Acceptor,Norm}}}} \{i | 1 \le i \le 3\} \quad (3)$$

Estimating pK_a^{app} values for ubiquitylation reactions. For UBE2N/UBE2V1, the pK_a^{app} values for synthetic UBs ($^{K63}UB_{C4}$ or $^{K63}UB_{C5}$) were measured by a steady-state kinetics assay that detects isopeptide bond formation between radiolabeled donor UB and unlabeled acceptor. First, a titration series was created using Bis-Tris propane buffer with pH values of 5.7, 6.1, 6.5, 6.9, 7.3, 7.7, 8.1, 8.5, 8.9, 9.3, 9.7 and 10.1. Stocks of Bis-Tris propane buffer, 10× reaction buffer (20 mM ATP, 10 mM DTT, 50 mM $MgCl_2$ and 500 mM NaCl), radiolabeled K63R donor UB, UBE2V1 and UBE2N (WT or K92R) proteins were added in the above order to autoclaved individual Eppendorf tubes. The final concentrations in the ubiquitylation reactions were 50 mM Bis-Tris Propane, 1× reaction buffer, 0.25 µM human UBA1, 5 µM radiolabeled K63R donor UB and 2 µM UBE2V1/K92R UBE2N complex. Following a 1-min incubation period, either synthetic $^{K63}UB_{C4}$ or $^{K63}UB_{C5}$ was added to initiate the reaction (100 µM final concentration). Reactions with $^{K63}UB_{C4}$ were quenched after 2 min and 45 s and reactions with synthetic $^{K63}UB_{C5}$ were quenched after 15 min in either non-reducing or reducing 2× SDS–PAGE buffer (100 mM Tris-HCl, pH 6.8, 20% glycerol, 30 mM EDTA, 4% SDS and 0.02% bromophenol blue). The reaction products and substrate were resolved by SDS–PAGE on 18% Tris-glycine polyacrylamide gels, followed by autoradiography and detection on a Typhoon 9410 Imager. Quantification of substrate and products was performed using Image Quant (GE Healthcare). The fraction of di-UB product for each reaction was measured by normalizing the signal for product over the total signal in the lane. These fractions were then multiplied by the donor UB concentration and divided by both the UBE2N/UBE2V1 complex concentration and the time of incubation. The velocities were plotted as a function of the pH of the reaction and fit to a sigmoidal four-parameter logistic curve with the Hill slope constrained to 1 (GraphPad Prism software, version 8.3). Note that this model assumes that the reaction velocities are dependent on a single ionizing species that becomes activated at high pH. A similar procedure was followed for UBE2R2 and $^{K48}UB_{C4}$ or $^{K48}UB_{C5}$, except for the following modifications. The final concentrations in the ubiquitylation reactions were 0.5 µM human UBA1, 15 µM radiolabeled K63R donor UB and 10 µM UBE2R2 protein. Reactions with $^{K63}UB_{C4}$ were quenched after 5 min and reactions with $^{K48}UB_{C5}$ were quenched after 60 min. The times of incubation were selected to ensure that all reaction velocities were within the linear range and that donor UB consumption was not sufficient to result in a lower concentration than E2. All reactions were performed in duplicate. All gels used in this experiment are shown in Source Data Table 1 and Source Data Extended Data Fig. 7.

Estimating the K_M for UBE2N/UBE2V1 complex. The K_M values of acceptor UBs were measured by a steady-state kinetics assay that detects isopeptide bond formation between radiolabeled donor UB and unlabeled acceptor. A 10× reaction buffer was prepared with 500 mM Bis-Tris propane, pH 7.3, 20 mM ATP, 10 mM DTT, 50 mM $MgCl_2$ and 500 mM NaCl. First, a twofold dilution series was established for acceptor UB proteins that had first been dialyzed into a buffer containing 30 mM Bis-Tris propane, pH 7.3. The starting concentrations of the dilution series were 1.4 mM for bacterial $^{K63}UB_{C4}$, 1.6 mM for synthetic $^{K63}UB_{C4}$ and 1.3 mM $^{K63}UB_{C5}$ (note that initiation of the reaction results in a further twofold dilution of each acceptor UB). Next, the following reagents were added from stock solutions to an Eppendorf tube to achieve final concentrations in each reaction of 1× reaction buffer, 0.25 µM human UBA1, 5 µM K63R donor UB and 2 µM UBE2N/UBE2V1 for bacterial or synthetic UB_{C4}, or 15 µM K63R donor UB and 10 µM UBE2N/UBE2V1 for $^{K63}UB_{C5}$. After a 2-min incubation period, aliquots of the master mix were evenly disbursed to clean Eppendorf tubes. Ubiquitylation reactions were then initiated by adding an equal volume of acceptor UB to the Eppendorf tubes containing the master mix. Reactions were incubated for either 15 or 30 min ($^{K63}UB_{C4}$ or $^{K63}UB_{C5}$, respectively) before quenching in either non-reducing or reducing 2× SDS–PAGE buffer containing 100 mM Tris-HCl, pH 6.8, 20% glycerol, 30 mM EDTA, 4% SDS and 0.02% bromophenol blue. The processing of reactions and estimation of velocities were performed as described in the previous section. The reaction velocities were fit to the Michaelis–Menten equation to estimate K_m (GraphPad Prism software, version 8.3). Reactions containing the RING domain of RNF4 were performed similarly with the following changes. All reactions contained 0.5 µM human UBA1, 15 µM K63R donor UB, 10 µM UBE2N/UBE2V1 and 1 µM RNF4. The starting concentrations of the dilution series were 1.3 mM for UB_{C4} and 1.25 mM for K63 UB_{C5}. Reactions were incubated for either 0.5 or 2.5 min (UB_{C4} or $^{K63}UB_{C5}$, respectively) before quenching. The times of incubation were selected to ensure that all reaction velocities were within the linear range and that donor UB consumption was not sufficient to result in a lower concentration than E2. Reactions were performed in duplicate. All gels used in this experiment are shown in Source Data Table 1.

Estimating the K_M for UBE2R2 and Rsp5p. The K_M values of acceptor UBs $^{K48}UB_{C4}$ and $^{K48}UB_{C5}$ for UBE2R2 and Rsp5p were measured similarly to the protocol described in the previous section with the following modifications. For UBE2R2, a twofold dilution series was established for acceptor UB proteins that had first been dialyzed into a buffer containing 30 mM Bis-Tris propane, pH 7.3 with starting concentrations of 8.4 mM for UB_{C4} and 12.5 mM for $^{K48}UB_{C5}$. The final concentrations in each reaction contained 0.5 µM human UBA1, 15 µM K48R donor UB and 10 µM UBE2R2 protein. Reactions were incubated for either 1 or 2.5 min for each replicate for the UB_{C4} titration series and for either 15 or 16 min for each replicate of the $^{K48}UB_{C5}$ titration series before quenching. For Rsp5p, the starting concentration of the acceptor UB dilution series was 1.6 mM for both UB_{C4} and $^{K63}UB_{C5}$. The final concentrations in each reaction contained 0.5 µM human UBA1, 7 µM K63R donor UB and 5 µM UBE2D2 and Rsp5p proteins. Reactions were incubated for either 5 or 30 min (UB_{C4} or $^{K63}UB_{C5}$, respectively) before quenching. The times of incubation were selected to ensure that all reaction velocities were within the linear range and that donor UB consumption

was not sufficient to result in a lower concentration than E2 or E3. Reactions were performed in duplicate. All gels used in this experiment are shown in Source Data Table 1.

Reporting Summary. Further information on research design is available in the Nature Research Reporting Summary linked to this Article.

Data availability

All raw gels are included in source data files. The MS proteomics data have been deposited to the ProteomeXchange Consortium via the PRIDE partner repository with the dataset identifier PXD021286. Source data are provided with this paper.

Code availability

ROSETTA software can be downloaded from www.rosettacommons.org and is available free to academic users.

References

51. Scott, D. C. et al. Two distinct types of E3 ligases work in unison to regulate substrate ubiquitylation. *Cell* **166**, 1198–1214 (2016).
52. Baek, K. et al. NEDD8 nucleates a multivalent cullin-RING-UBE2D ubiquitin ligation assembly. *Nature* **578**, 461–466 (2020).
53. Brown, N. G. et al. Mechanism of polyubiquitination by human anaphase-promoting complex: RING repurposing for ubiquitin chain assembly. *Mol. Cell* **56**, 246–260 (2014).
54. Plechanovova, A. et al. Mechanism of ubiquitylation by dimeric RING ligase RNF4. *Nat. Struct. Mol. Biol.* **18**, 1052–1059 (2011).
55. Sievers, Q. L. et al. Defining the human C2H2 zinc finger degrome targeted by thalidomide analogs through CRBN. *Science* **362**, eaat0572 (2018).
56. Weissmann, F. et al. biGBac enables rapid gene assembly for the expression of large multisubunit protein complexes. *Proc. Natl Acad. Sci. USA* **113**, E2564–E2569 (2016).
57. Duda, D. M. et al. Structural insights into NEDD8 activation of cullin–RING ligases: conformational control of conjugation. *Cell* **134**, 995–1006 (2008).
58. Ziemba, A. et al. Multimodal mechanism of action for the Cdc34 acidic loop: a case study for why ubiquitin-conjugating enzymes have loops and tails. *J. Biol. Chem.* **288**, 34882–34896 (2013).
59. Rappsilber, J., Ishihama, Y. & Mann, M. Stop and go extraction tips for matrix-assisted laser desorption/ionization, nanoelectrospray and LC/MS sample pretreatment in proteomics. *Anal. Chem.* **75**, 663–670 (2003).
60. Kulak, N. A., Pichler, G., Paron, I., Nagaraj, N. & Mann, M. Minimal, encapsulated proteomic-sample processing applied to copy-number estimation in eukaryotic cells. *Nat. Methods* **11**, 319–324 (2014).

Acknowledgements

This study is dedicated the memory of our inspiring mentor, colleague and beloved friend, Huib Ovaa, whom we miss dearly. We thank J.R. Prabu, J. Kellermann, S. von Gronau, D. Scott, S. Uebel, S. Pettera, V. Sanchez, K. Baek, D. Horn-Ghetko and S. Kostrhon for assistance, reagents and helpful discussions. We also thank C. Talavera-Ormeño and P. Hekking for assistance with peptide synthesis. B.A.S. has received funding from the European Research Council (ERC) under the European Union's Horizon 2020 research and innovation programme (grant no. 789016-NEDD8Activate), and from the Deutsche Forschungsgemeinschaft (DFG, German Research Foundation—SCHU 3196/1-1). B.A.S. and M.M. are supported by the Max Planck Society. Also, N.P., D.H., N.B. and G.K. were supported by a grant from the National Institutes of Health (R15GM117555-02). G.J.v.d.H.v.N was supported by grants from NWO (VIDI and Off-Road). H.O. was supported by a VICI grant from the Netherlands Foundation for Scientific Research (NWO). Work by M.S. and M.J.B. was performed within the framework of SFB 1035 (German Research Foundation DFG, Sonderforschungsbereich 1035, no. 201302640, project Z01).

Author contributions

Syntheses of UB analogs were designed and executed by G.J.v.d.H.v.N. J.L. performed all biochemical assays. Kinetics experiments were carried out by G.K., N.P., D.H. and N.B. MS experiments were designed and conducted by M.M., F.M.H. and O.K. MD simulations were performed by V.H.T. and J.S.H. NMR was carried out by M.J.B. and M.S. The manuscript was prepared by J.L., D.T.K., G.J.v.d.H.v.N., G.K., H.O. and B.A.S., with input from all authors. The project was supervised by B.A.S., G.K., H.O. and D.T.K.

Competing interests

H.O. was a shareholder of UbiqBio. All other authors declare no competing interests.

Additional information

Extended data is available for this paper at https://doi.org/10.1038/s41589-020-00696-0.

Supplementary information is available for this paper at https://doi.org/10.1038/s41589-020-00696-0.

Correspondence and requests for materials should be addressed to G.K., H.O. or B.A.S.

Reprints and permissions information is available at www.nature.com/reprints.

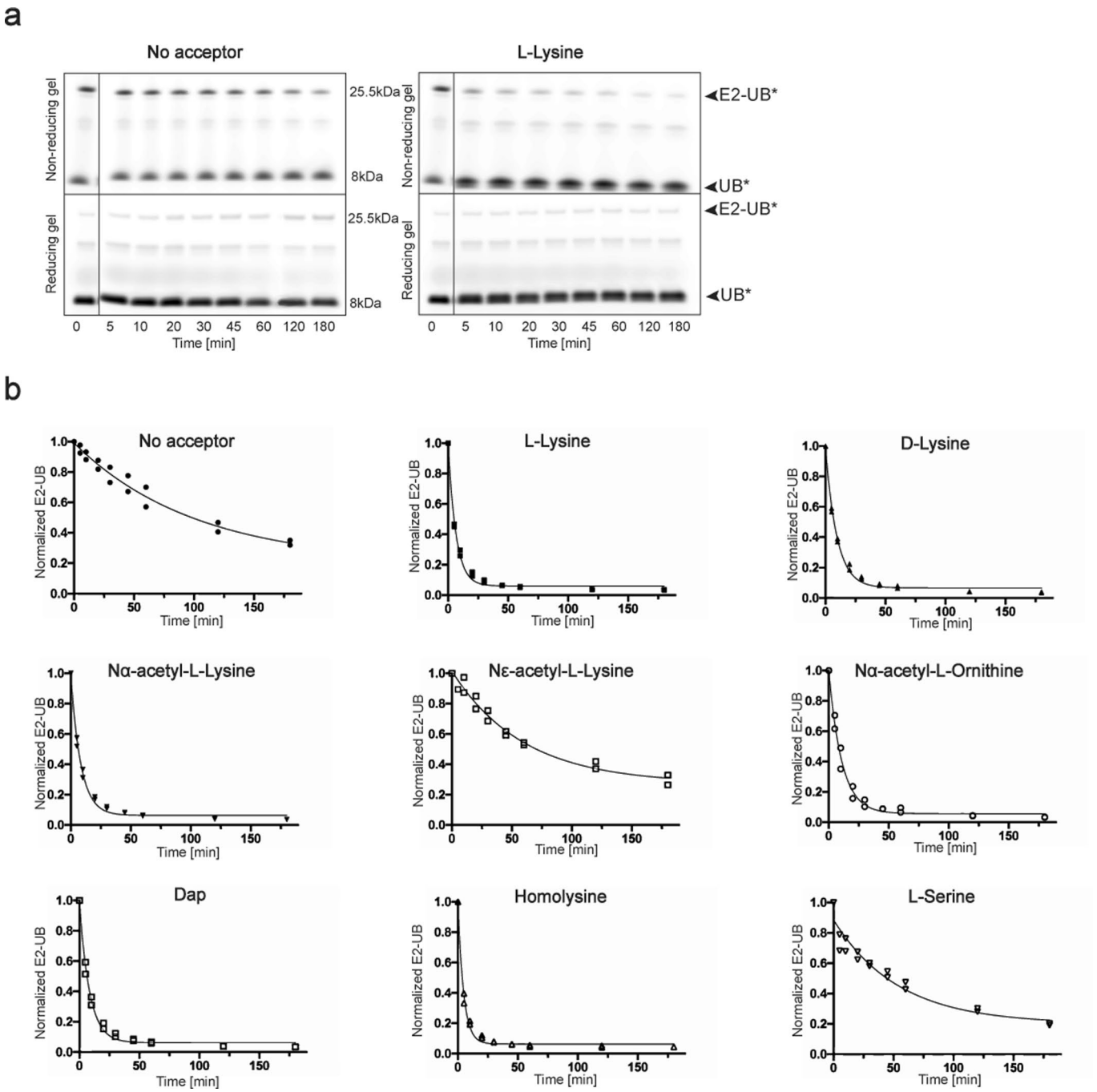

Extended Data Fig. 1 | UBE2N~UB/UBE2V1/RNF4 RING E3 complex reacts preferentially with free amino acids harboring amine acceptors and various side-chain. a, Fluorescence scan of SDS-PAGE gels demonstrating the discharge of labeled UB (UB*) to L-lysine compared with the absence of amino acid acceptor using wild-type UBE2N. Electrophoresis was performed under both reducing and non-reducing conditions to differentiate thioester bonded complexes from isopeptide bonded E2-donor UB ones. **b**, Time-courses of fluorescent UB discharge from UBE2N K92R~UB/UBE2V1/RNF4 RING E3 to the indicated amino acids, normalized to starting signal of fluorescent UB thioester-bonded to UBE2N. For all, N=2 independent experiments. For samples derived from the same experiment, gels were processed in parallel.

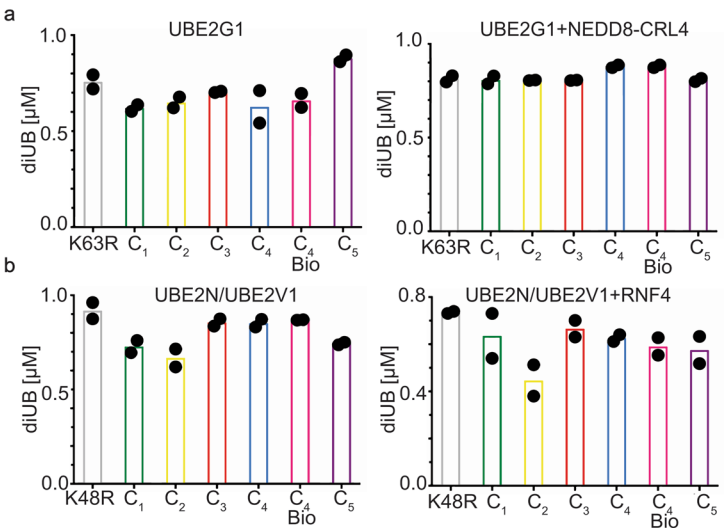

Extended Data Fig. 2 | K48 and K63 chain-forming E2s equally discharge to $^{K63}UB_{C1\text{-}C5}$ and $^{K48}UB_{C1\text{-}C5}$ acceptors respectively. a, Di-UB formed by K48 UB chain-forming E2 UBE2G1 with $^{K63}UB_{C1\text{-}C5}$ acceptors in the absence (left) or presence (right) of neddylated CRL4 (N8CRL4). **b**, Di-UB formed by the K63 UB chain-forming E2 UBE2N/UBE2V1 complex with the $^{K48}UB_{C1\text{-}C5}$ acceptors in the absence (left) or presence (right) of the E3 RNF4 RING domain. For all plots graphs, di-UB levels (μMol) represent the final time-points from the reactions (Source Data Extended Data Fig. 2), N=2 independent experiments. For samples derived from the same experiment, gels were processed in parallel.

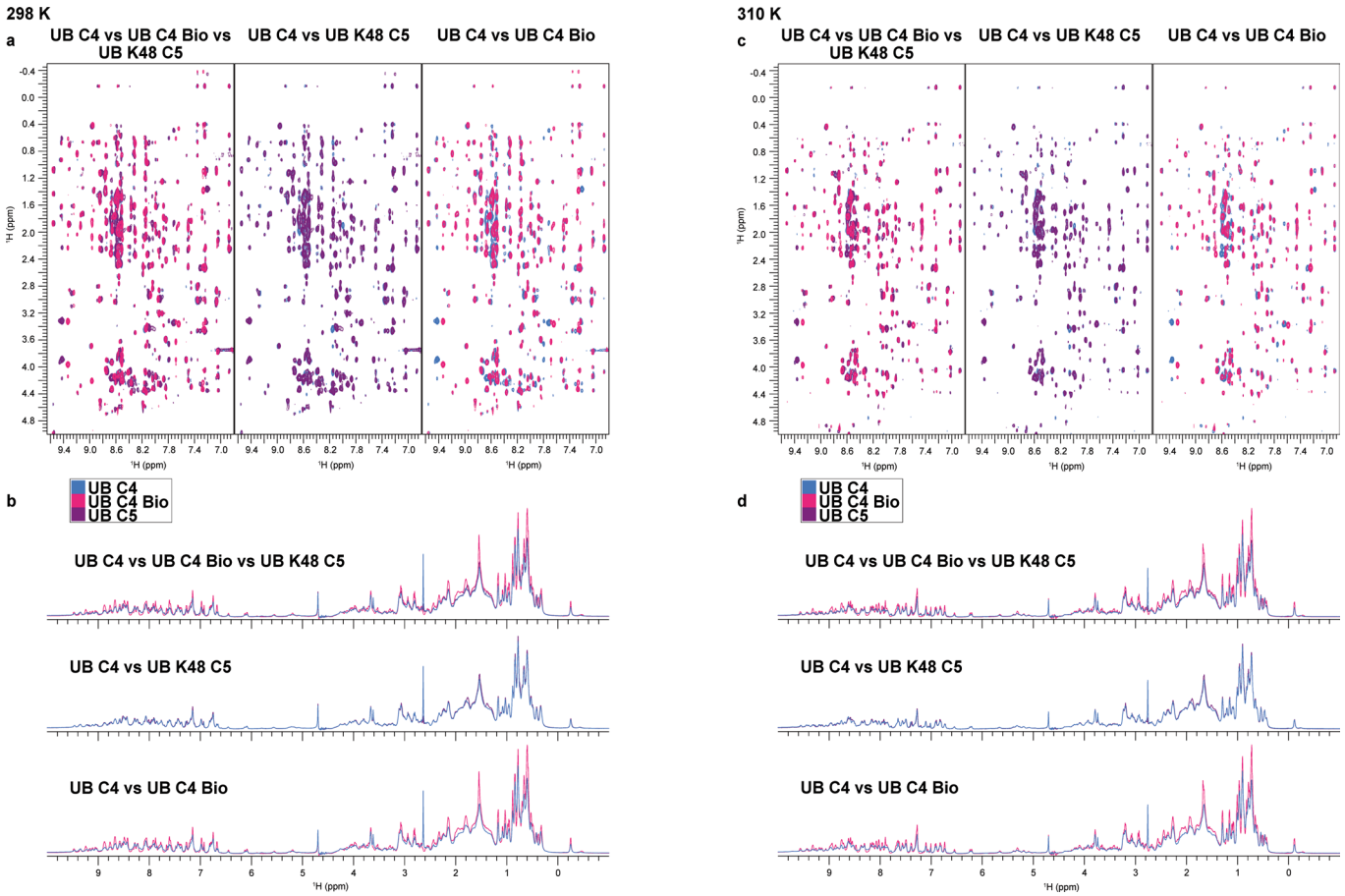

Extended Data Fig. 3 | 1D and 2D proton NMR spectra for synthetic UB_{C4}, recombinant UB, and $^{K48}UB_{C5}$ are highly superimposabe. a, 2D Nuclear Overhauser effect spectroscopy (NOESY) recorded at 298 K and 1D spectra (**b**) for UB_{C4} (blue), recombinant UB (C4 Bio; pink) and $^{K48}UB_{C5}$ (purple). The 2D NOESY spectra show NOE interactions between amide protons (x-axis) and amino acid side-chain protons (y-axis), whereas the 1D spectra show signals from methyl protons (-0.5–1.0 ppm), Cα-protons (3.5 – 6 ppm) and amide protons (6 – 10 ppm). The signal from water is at 4.7 ppm[1]. The observed dispersion of signals demonstrates that all three UBs are well folded, while the comparable overlays indicate that the UBs share a highly similar fold. **c**, same as (**a**), except data were recorded at 310 K. **d**, same as (**b**), except at 310 K.

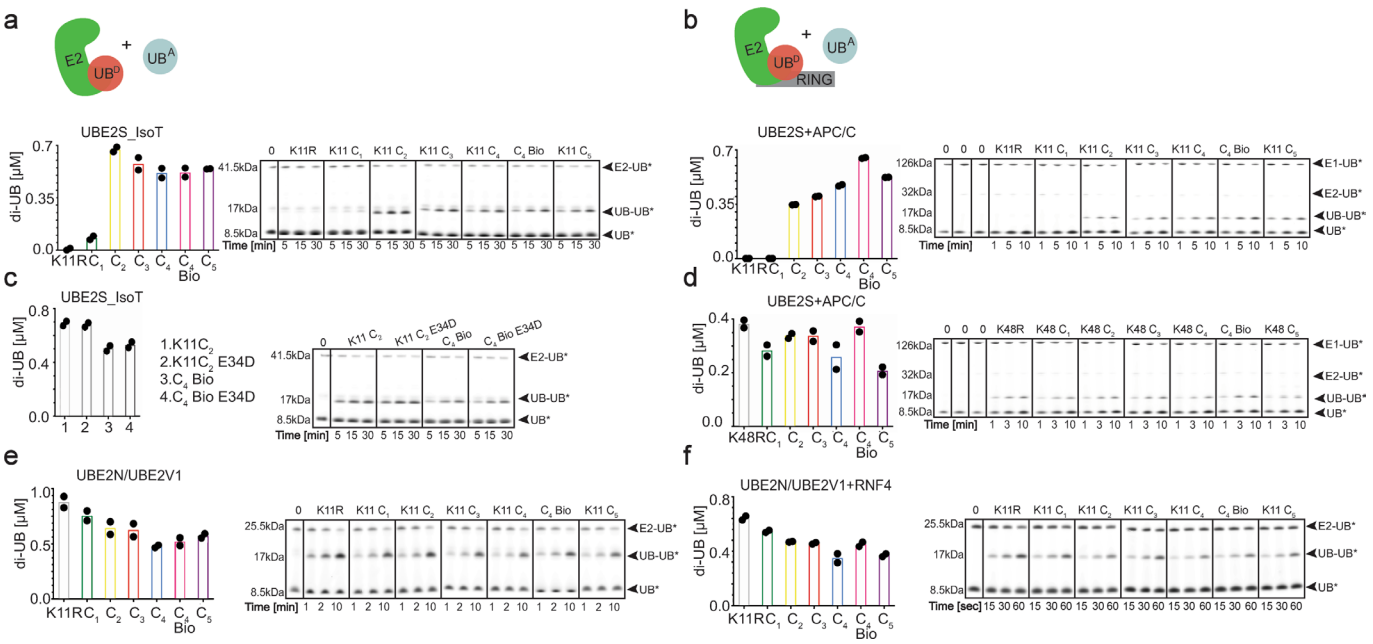

Extended Data Fig. 4 | Lack of preference for a native lysine on acceptor UBs for the K11 chain-forming E2 UBE2S. a, Cartoon of experimental scheme monitoring the reactivity of E2s with $^{K11}UB_{C1\text{-}C5}$ acceptors (UB^A). Plot of the discharge of labeled UB (UB*) from UBE2S_IsoT to ^{K11R}UB, $UB_{C4\ Bio}$ or $^{K11}UB_{C1\text{-}5}$ acceptors (left) and representative fluorescence scans of SDS-PAGE gels representing the primary data (right). **b**, same as (**a**), except in the presence of the E3 APC/C. **c**, same as (**a**), except in the presence of $^{K11}UB_{C2}$ or $UB_{C4\ Bio}$ acceptors or the same harboring an E34D mutation. **d**, same as (**b**), except in the presence of ^{K48R}UB, $UB_{C4\ Bio}$ or $^{K48}UB_{C1\text{-}5}$ acceptors. **e**, same as (**a**), except with UBE2N/UBE2V1. **f**, same as (**b**), except with UBE2N/UBE2V1 and the RING domain from the E3 RNF4. For all plots graphs, di-UB levels (μMol) represent the final time-points from the reactions (N=2 independent experiments). For samples derived from the same experiment, gels were processed in parallel.

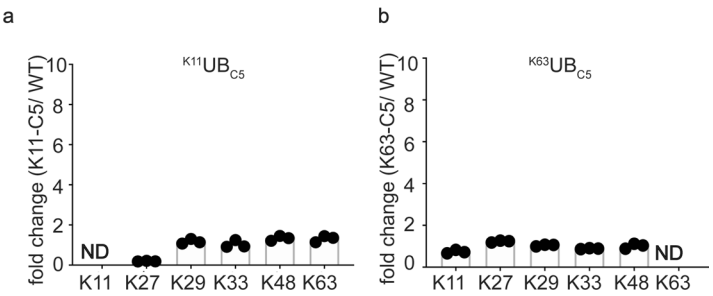

Extended Data Fig. 5 | The location of lysine analogues on acceptor UB impacts the distribution of di-UB chain linkage types generated by the E2 enzyme UBE2D3. a, Plots showing the relative changes in UBE2D3 generated di-UB chain linkages in the presence of the RING domain from the E3 RNF4, comparing products containing $^{K11}UB_{C5}$ or UB_{C4} acceptors (N=3 technical replicates). ND, not determined. **b**, Same as (**a**), except with $^{K63}UB_{C5}$ acceptor.

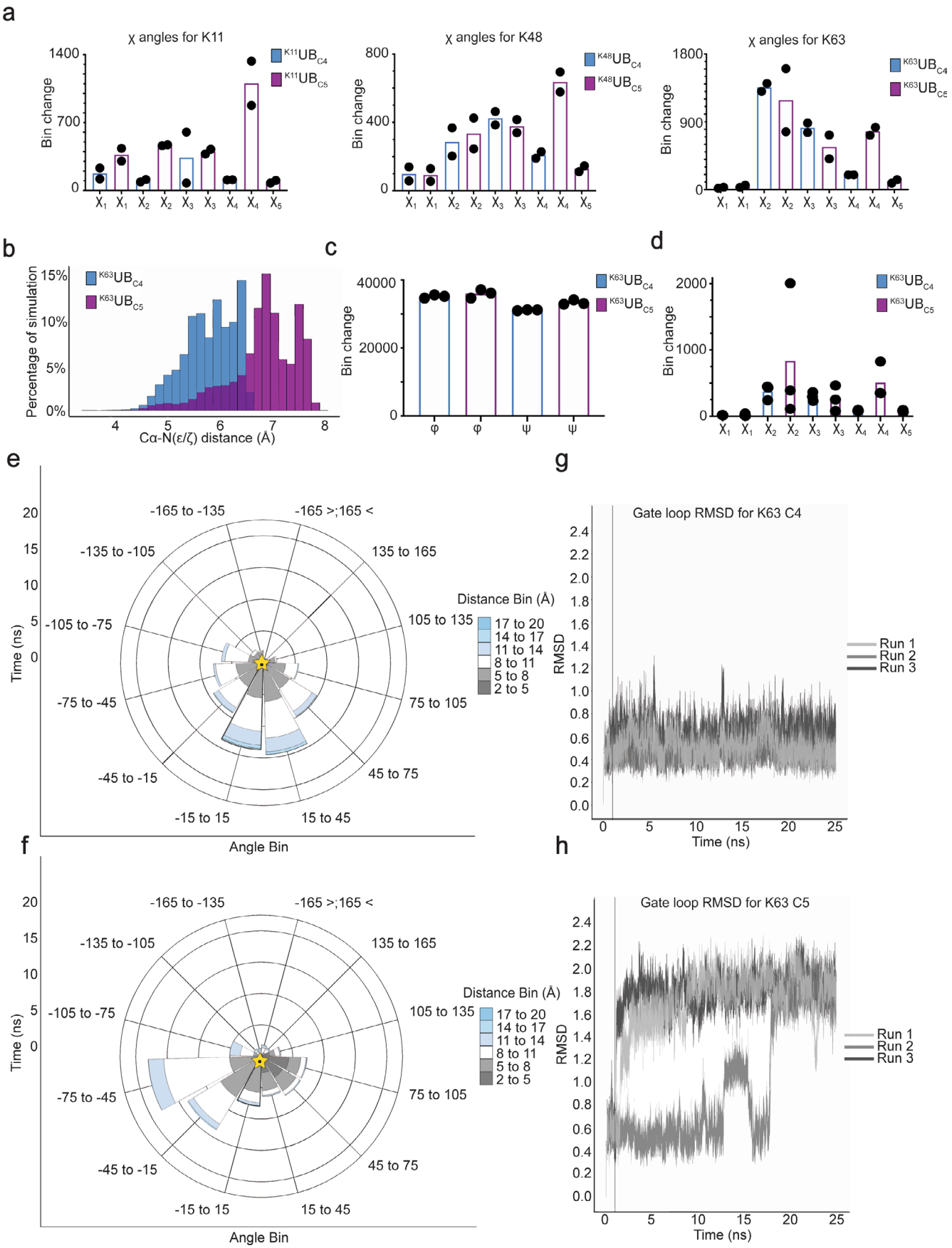

Extended Data Fig. 6 | See next page for caption.

Extended Data Fig. 6 | Molecular Dynamics simulations reveal pleiotropic structural effects on UBs harboring lysine analogs. a, Plot showing the degree of various side-chain rotamer interconversions for $^{K11}UB_{C5}$, $^{K48}UB_{C5}$, or $^{K63}UB_{C5}$ versus UB_{C4} acceptor UBs. Bins are divided by 120° intervals. **b**, Distribution of the distances between lysine acceptor amine and Cα atoms for UB_{C4} versus UB_{C5} during 25 ns MD simulations (N=3 independent experiments) for the UBE2N~UB/UBE2V1/acceptor UB multi-subunit complex. Bins are divided by 10° intervals. **c**, Plot showing the dynamics of φ and ψ main-chain torsion angles for UB_{C4} or UB_{C5} acceptors in the UBE2N~UB/UBE2V1/acceptor UB multi-subunit complex. Bins are divided by 10° intervals. **d**, Plot showing the dynamics of the side-chain rotamers for UB_{C4} or UB_{C5} acceptors in the UBE2N~UB/UBE2V1/acceptor UB multi-subunit complex. Bins are divided by 120° intervals. **e**, Rose plot showing the distance and angle of the amine acceptor of UB_{C4} relative to the active-site during 25 ns MD simulations of the UBE2N~UB/UBE2V1/acceptor UB multi-subunit complex (N=3 independent experiments). Golden star indicated starting position. **f**, same as (**e**), but with $^{K63}UB_{C5}$ (**g**) RMSD of gate loop during the trajectory for UB_{C4}. **h**, same as (**g**), except with $^{K63}UB_{C5}$.

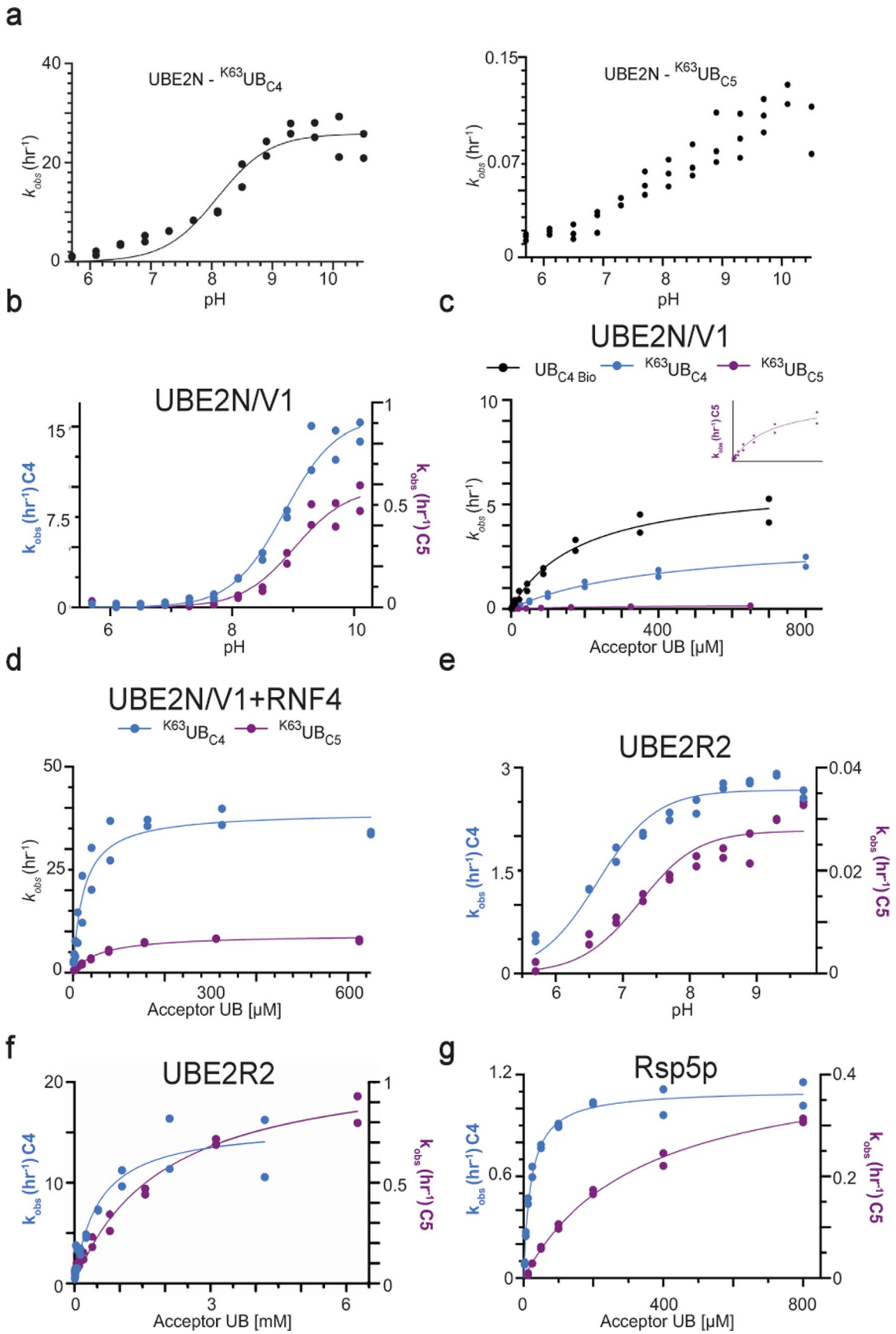

Extended Data Fig. 7 | See next page for caption.